Cone photoreceptor heterogeneity in the primate retina

Jacob Alexander Baudin

A dissertation

submitted in partial fulfillment of the

requirements for the degree of

Doctor of Philosophy

University of Washington

2018

Reading Committee:

Frederick M. Rieke, Chair

Greg Horwitz

Jay Neitz

Program Authorized to Offer Degree:

Physiology and Biophysics

University of Washington

Abstract

Cone photoreceptor heterogeneity in the primate retina

Jacob Alexander Baudin

Chair of the Supervisory Committee:
Professor Frederick M. Rieke
Department of Physiology and Biophysics

Human vision commences when light is transduced to a neural signal. In daylight, this occurs predominantly within cone photoreceptors. Does this transduction occur identically for all light inputs? The work in this thesis addresses this question as well as the role of phototransduction in controlling downstream signals in the visual system. Chapter 2 focuses on heterogeneity in the transduction of light across wavelengths due to differences in short-, medium-, and long-wavelength sensitive cone photoreceptors. Chapter 3 elaborates on heterogeneity in transduction of inputs across visual space arising from differences in cones across retinal eccentricity. Chapter 4 begins to explore an instance where cone signals directly control retinal output. Together, this body of work aims to provide an appreciation for heterogeneity in signal transduction within cones throughout the primate retina and link cone properties to both retinal output and perception.

TABLE OF CONTENTS

LIST OF FIGURES

ACKNOWLEDGEMENTS

Many people are owed thanks for their contributions to the production of this thesis.

It is challenging to articulate the impact Fred has had both on this work as well as my growth during graduate school. Fred's commitment to mentoring is unique. He remains one of the most experimentally active members of the lab and sets an example with his genuine curiosity and continuous insight. This is far from the only example he sets. Fred expertly demonstrates success in balancing a commitment to science with that to his family and priorities outside of research. While my time as his formal mentee is drawing to a close, I know he deserves preemptive acknowledgement for the fact that he will remain a guiding example I will look to of one who enjoys and balances a successful career and life in a manner that appears so effortless.

Fellow members of the Rieke Lab have made it a great place to spend my years in graduate school, both scientifically and otherwise. Raunak Sinha deserves special mention for being a great collaborator on all work involving foveal and peripheral retina. I have been fortunate to spend my time (potentially too much of it not doing work...) sitting in an office filled with friends and colleagues: Ali Weber, Phil Mardoum, Greg Newkirk, Max Turner. Many others (both in the Rieke Lab and elsewhere) have provided valuable advice and mentoring throughout my time in the lab: Mike Manookin, Sid Kuo, Will Grimes, Juan Angueyra, Gabrielle Gutierrez, Braden Brinkman, Zhou Yu. The lab's work is greatly aided by the work of Mark Cafaro, Shellee Cunnington, and Mike Ahlquist.

My thesis committee, consisting of Greg Horwitz, Adrienne Fairhall, Jay Neitz, Maureen Neitz, and Bill Zagotta provided valuable advice as I completed this work. Greg Horwitz deserves special mention for going above and beyond in providing thoughtful feedback on my projects as well as in multiple instances when I have presented my work in written form.

Our work in primate retina would not be possible without the Washington National Primate Research Center's Tissue Distribution Program, and specifically the efforts of Chris English and Drew May.

I would like to thank my family and friends. I am very fortunate to have been able to attend graduate school, an opportunity that would not have been possible without the irreplaceable support and encouragement of my parents and siblings in developing and nurturing my interest in learning. And finally, I would like to thank Shahaf - and endless source of support and love in all I choose to do.

Chapter 1. INTRODUCTION

Although we are rarely acutely aware of failures in our perception, it has long been appreciated that our perceptual abilities fall short of perfection. This is exploited in the design of numerous devices we interact with on a daily basis. A simple yet ubiquitous example is fluorescent light bulbs powered by alternating current circuits. The intensity of light emitted from these bulbs varies with a frequency matched to that of the current, but this is a generally imperceptible phenomenon. Similarly, videos on phones, computers, and televisions are composed of a series of static images that rapidly update on a screen. With modern devices, this sequence of images becomes indistinguishable from actual movement. For decades following the advent of motion pictures, frames were cycled through at a slower rate and transitions between them were perceptible. The fact that individual frames are not perceived in modern movies suggests that, as frame rates increase, our perception transitions from successfully detecting that a movie is not truly continuous motion to a realm in which it is unable to do so.

What is the origin of limits on our perception? Answers to this question come through understanding the processes by which we perceive our environments. Sensory systems are the parts of our nervous systems that provide an interface with the physical world, and therefore form the basis of our perception. Our perceptions and interactions with our environments rely exclusively on information collected by these neural circuits. How well do they detect the range of physical stimuli in the external world? Significant efforts have been made to understand both the remarkable tasks they accomplish as well as the situations in which they fail to detect important aspects of our environments.

Establishing correspondences between the performance of our perception and the function of the underlying neural circuits is a major goal of sensory neuroscience. Failures of perception often play an important role in this process because understanding what our perceptual systems can accomplish and what they cannot is often quite instructive. When perception fails, there must be a neural mechanism failing to accurately detect or transmit information about some aspect of the environment. Armed with this knowledge, sensory neuroscientists can constrain models of how the underlying neural circuits must function and make targeted efforts to experimentally probe the mechanistic basis of these failures. Further, when the study of neural circuit elements shows that they contain more information than is available perceptually, it necessitates that information must be lost in downstream steps. The successes of our perceptual systems can be equally informative because information about anything we can perceive must be present in the responses of cells within our sensory systems. Work motivated by perceptual phenomena often advances our understanding of neural circuits beyond simply explaining a specific perceptual phenomenon, and contributes to an overall improved understanding of circuit function.

Exploiting connections between perception and the function of neural circuit elements is an effective framework that is frequently used to study sensory systems. The work presented in this thesis will take such an approach to exploring primate visual system function at multiple points within the retina. A unifying theme will be developing a better understanding of the function of cone photoreceptors and the role they play within retinal processing. Results from these inquiries will be related to corresponding limits placed on primate visual perception.

1.1 Signal Detection Initiates Perception

Sensory systems mediate organisms' interactions with their environments by providing their nervous systems with information about the physical world. In every sensory system, this process

begins when some aspect of the physical world is converted to a neural signal. In the visual system, a biochemical cascade in rod and cone photoreceptors transduces photon arrival into a change in membrane current and ultimately neurotransmitter release (Baylor, 1996). In the olfactory system, extracellular receptors detect the presence of different small molecules, which again is translated into a change in neurotransmitter release (Ronnett & Moon, 2002). Other sensory modalities detect oscillations in air pressure, pressure on skin, or small molecules in food. Although each of these sensory systems provides information about a different aspect of the physical world, an initial signal detection (or sensory transduction) step is always present.

As the initial step in perception, signal detection provides all of the information to which a sensory system has access. An organism's nervous system will never have access to information about any aspect of the environment that its signal detectors cannot transduce. In this way, the properties of sensory signal detectors place fundamental limits on which aspects of the physical world an organism can interact with, and represent the first point at which a sensory system can fail. There are many examples across sensory systems where limits imposed by signal detection are readily apparent. For instance, although the electromagnetic spectrum contains photons with wavelengths ranging from picometers to thousands of kilometers, the primate visual system is only capable of perceiving those whose wavelengths are between approximately 400 and 700 nanometers (Baylor *et al.*, 1987). Similarly, the primate auditory system is only capable of detecting vibrations in air pressure at frequencies ranging from approximately 20 to 20,000 Hz, although pressure vibrations regularly occur at frequencies outside this range (Kandel *et al.*, 2013). In either case, information about our physical environment falling outside of a detectable range never enters our nervous system and thus is absent in perception.

A particularly elegant example of a direct correspondence between signal detection and perceptual limits occurs at very dim light levels in the primate visual system (Field *et al.*, 2005). Under these conditions, rod photoreceptors are the principal signal detectors. For decades it has been known that the primate visual system must be capable of detecting the absorption of a single photon in a rod (Hecht, 1942; Baylor *et al.*, 1979, 1984; Tinsley *et al.*, 2016). Nonetheless, there is still trial to trial variability in whether or not an observer can perceive such a stimulus. When stimulated with very weak flashes under dim lighting conditions, the presence of a response in rods appears to follow Poisson statistics, which is expected based on the physical properties of light. Similarly, the variability in an observer's detection of these dim flashes can also be shown to be governed by Poisson statistics. Ultimately, an observer can never perceive such stimuli if they do not generate signals in their rods, and the ability of rods to generate a signal is limited by statistical fluctuations in photon absorption. This tight link between signal detection and perceptual performance demonstrates the significant role the properties of signal detectors play in sculpting and limiting our perception.

Understanding signal transduction within a sensory system is an important first step in both understanding that system's function and in explaining perception. It is useful for multiple reasons. For example, many studies of sensory systems aim to understand the computations performed at different levels of the underlying neural circuitry. This generally involves recording a cell's responses to a set of stimuli and attempting to describe its input-output relationship. Often, the inputs are taken to be the physical stimuli. Describing the computations underlying a downstream cell's responses as acting on physical inputs neglects the fact that there is significant processing performed at the level of signal detection as well as throughout downstream steps. Having an accurate understanding of a sensory system's signal detection process allows researchers of

downstream circuit elements to better predict the inputs to the specific cell they are studying. Furthermore, as is the case with single photon detection by primates, perceptual limits can often be directly related to limits in signal detection. Understanding signal detection allows human perception to be better explained. Establishing these correspondences can be helpful by placing strong constraints on the function of the circuitry transforming detected signals to perception. For example, knowing that human perceptual sensitivity under dim lighting conditions approaches limits set by noise in rod photoreceptors places strong constraints on the operation of the circuits reading out their signals. These constraints have proven extremely useful in guiding the investigation of these circuits (Field *et al.*, 2005).

1.2 Signal Detection By Photoreceptors in the Visual System

Photons are detected in the visual system by two types of photoreceptors, rods and cones. As previously discussed, rod photoreceptors operate under dimmer lighting conditions, while detection under brighter conditions is performed by cone photoreceptors. These photoreceptors are a specialized class of cells containing the machinery necessary to transduce photon arrival into a change in membrane voltage, and therefore neurotransmitter release. Both rods and cones rely on a relatively conserved biochemical pathway, called phototransduction, to perform this transduction process (Figure 1.1, reviewed in Yau and Hardie 2009).

In darkness, photoreceptors are depolarized with a continuous current (dark current) flowing across their membranes. This current flows through cGMP-gated cation channels that remain open in the presence of cGMP and close in its absence. In darkness, steady-state cGMP levels open a sufficient number of these channels to place photoreceptors in a depolarized state in which they tonically release glutamate. Phototransduction links photon absorption to a reduction in cGMP, thereby closing cGMP-gated channels, hyperpolarizing the cell, and decreasing

glutamate release. The transduction process begins when a photon is absorbed by a transmembrane opsin protein. Opsins are members of the G-protein coupled receptor family and conjugate a small molecule, retinal, that isomerizes from 11-cis retinal to all trans retinal upon the absorption of a photon. This isomerization produces a conformational change in the opsin protein, causing it to activate the G-protein transducin. Transducin proceeds to activate phosphodiesterase (PDE) enzymes, which cleave cGMP molecules to produce GMP. The subsequent reduction in glutamate release following a decrease in cGMP levels and the resulting closure of cGMP-gated channels completes the process of converting photon arrival into a neural signal.

In addition to the feedforward biochemical cascade of phototransduction, there are feedback mechanisms that further sculpt photoreceptor responses. Changes in intracellular calcium mediate many of these mechanisms and are controlled by two competing processes (Yau & Hardie, 2009). Calcium enters the cell as a small fraction of the cGMP-gated channel current, and is extruded by a Na/Ca, K exchanger. When photon absorption causes a reduction in the dark current, there is a decrease in calcium influx and therefore intracellular calcium levels. Falling calcium levels mediate negative feedback at multiple stages in the phototransduction cascade. First, decreased calcium causes an increase in G protein-coupled receptor kinase (GRK) activity. GRK phosphorylates opsin proteins and reduces their active lifetime. Second, a drop in calcium causes increased cGMP production by increasing the activity level of guanylate cyclase, the enzyme producing cGMP from GTP. This effect is mediated through calcium's interaction with guanylate cyclase activating proteins. Finally, calcium interacts with the cGMP-gated channels themselves and reduces their affinity for cGMP. Therefore, when calcium levels are reduced, the channel affinity for cGMP rises. Together these mechanisms help regulate the phototransduction process.

1.3 Rod and Cone Photoreceptor Function

While both rods and cones employ the same general phototransduction cascade, molecular differences in the components of their pathways leave them specialized to detect different aspects of the visual world (Miller *et al.*, 1994). These differences exemplify a common occurrence in sensory systems; the input-output relationships of their components are often matched to the specific inputs they are encoding (Laughlin, 1981). Furthermore, cells often dynamically change their input-output transformation as the statistics of their relevant inputs change (Fairhall *et al.*, 2001). Investigations of primate rod and cone function have shown that both classes of photoreceptors demonstrate these properties.

Rods provide reliable signals under dim lighting conditions and their properties are matched to the task they perform. To this end, their response per absorbed photon is quite large and they have low noise in their signals (Baylor *et al.*, 1979, 1984). This allows them to be sensitive enough to reliably signal the absorption of a single photon. One cost of their high sensitivity is that they saturate at low light levels. To mitigate this, they adapt the size of their responses across their operational range to better match their encoding to their inputs (Baylor *et al.*, 1984). An additional cost associated with their heavily amplified responses is that they are relatively slow, which places limits on their ability to respond to signals undergoing rapid temporal modulation. For example, under rod-mediated conditions, human observers are unable to detect flickering stimuli above approximately 15 Hz (Hecht & Shlaer, 1936).

Cones play a complementary role in the visual system, and provide its main inputs under daylight conditions. In this capacity, they are optimized to operate at brighter light levels over a range of stimuli many orders of magnitude larger than that of rods. Their responses are faster, smaller, and noisier (Schnapf *et al.*, 1990). Although these response properties leave them unable

to reliably signal the arrival of single photons, it allows them to operate over an impressively broad range of light levels and produce responses to signals modulated much more rapidly in time. In contrast to rod-mediated vision, under cone-mediated conditions human observers can detect flickering stimuli at frequencies exceeding 80 Hz (Tyler, 1987).

Given the breadth of visual stimuli that are physically realizable within their operating range, it is impossible for a cones to simultaneously be able to effectively encode them all. Instead, their input-output relationship at any instant will always be better suited for encoding certain stimuli compared to others. To dynamically optimize their stimulus encoding to match the statistics of these diverse inputs, cone response properties undergo significant adaptation.

Cone adaptation has been studied extensively due to its importance in affording them their broad operating range (Valeton & van Norren, 1983; Schnapf *et al.*, 1990; Schneeweis & Schnapf, 1999). Adaptation adjusts cones' input-output relationships by changing response properties such as the amplitude and kinetics (Figure 1.2A). For example, different response amplitudes are better suited for signaling under different input conditions. If cone response amplitudes remained constant across backgrounds, they would risk either saturating under bright lighting conditions, or failing to respond under dim conditions. Instead, their response size per absorbed photon decreases as background light levels increase. This enhances their ability to provide information about fluctuations around the mean light level, but there are always trade-offs with such a process. For example, by having larger responses at dim light levels, they are prone to saturate if an extremely bright stimulus occurs on a dim background. Nonetheless, these adaptive changes have been shown to be well matched to natural scene statistics, where mean light level and contrast tend to be statistically independent (Mante *et al.*, 2005). Another aspect of cone responses that adapts is their kinetics; cone signals become faster as background light levels increase (Rieke & Baylor, 2000;

Dunn *et al.*, 2007). With this speeding, their ability to encode rapidly varying stimuli improves as light levels increase.

Response amplitude and kinetics are properties of the signals generated by cones, but noise in their responses also has a significant bearing on their performance as signal detectors. As discussed, statistical fluctuations in photon absorption place initial limits on our perception (Geisler, 1989). Following this, noise within cone photoreceptors places another of the earliest limits on our visual system. Phototransduction is composed of a series of biochemical reactions, all of which have some degree of stochasticity. In primate cones, noise arises from multiple stages in the phototransduction cascade (Angueyra & Rieke, 2013). For example, spontaneous activation of opsin or phosphodiesterase molecules causes fluctuations in the cone membrane current. Understanding noise in primate photoreceptors has begun to contribute to explaining perceptual limits because it is ultimately their signals in the context of their noise that limits their performance, and therefore perception. Improving our understanding of both their signals and noise will allow further connections to be drawn between their properties and perception.

1.4 Cone Photoreceptor Heterogeneity

In trichromatic primates, there are three distinct classes of cone photoreceptors with unique spectral sensitivities: S (blue sensitive) cones, M (green sensitive) cones, and L (red sensitive) cones (Figure 1.3). Comparisons between signals originating in these different cone types forms the basis of color vision (Shevell, 2003).

Classically, it has been accepted that these differences in spectral sensitivity are the only major difference between primate cones, and that the response to an equivalent number of absorbed photons would be identical across all cones in the primate retina (Schnapf *et al.*, 1990). Initial recordings from small sets of peripheral primate cone photoreceptors supported the assumption

that the only difference between L, M, and S cones was their spectral sensitivity. This assumption of homogeneity across primate cones has persisted despite work in other species, such as salamander and goldfish, showing significant differences in the responses generated by different cone types (Rieke & Baylor, 2000; Howlett *et al.*, 2017).

The properties of primate cones described above were studied mainly in L and M cones in the peripheral retina. This is because cones were assumed to be functionally homogeneous and peripheral L and M cones are the most experimentally accessible. Interestingly, it was recently shown that there are significant differences in responses of cones across eccentricity (Sinha *et al.*, 2017). L and M cones in the fovea, the central-most part of the retina providing our highest acuity spatial and color vision, generate responses that are significantly slower than those generated by cones in peripheral retina (Figure 1.2B). This finding demonstrates that there are functionally distinct populations of cones in primate and underscores the importance revisiting assumptions about cone homogeneity.

Heterogeneity in the response properties of different cone photoreceptors is significant because it directly translates into heterogeneity in signal detection within our visual system, and ultimately perception. Chapter 2 explores differences we have found in the signaling properties of primate S cones versus L and M cones. Building upon the initial differences in cones across eccentricity presented by Sinha et al., 2017, Chapter 3 develops a more comprehensive understanding of differences in primate cones across space.

1.5 The Primate Retina

The retina consists of many convergent and divergent parallel pathways. Comprising these pathways in mouse, for example, are over 80 different cell types (Sanes & Masland, 2015). In both mouse and primate, these numerous cell types fall into 5 main classes of cells arranged in a

common structural motif (Figure 1.4). In the canonical feedforward pathway, rod and cone photoreceptors synapse onto bipolar cells. Bipolar cells synapse onto retinal ganglion cells, whose axons make up the optic nerve carrying signals to higher visual centers. These feedforward signals are sculpted by lateral interactions at two main sites. Horizontal cells carry lateral signals at the level of the photoreceptor to bipolar cell synapse, as do amacrine cells at the level of the bipolar cell to retinal ganglion cell synapse. These lateral interactions add an extra level of complexity to the computations that can be implemented by the retinal circuitry.

Circuits in the retina process and extract information from cone signals before sending them to the brain. Just as the properties of cones have major implications for our perception, so do those of the downstream circuitry carrying their signals. Our perception is shaped by the combined properties of transduction by photoreceptors as well as the processing and transformation performed by downstream circuitry. In many cases, these processes work together to accomplish a given task.

Adaptation in the peripheral primate parasol and midget ganglion cell pathways is a particularly salient example of complementary roles of different circuit elements (Dunn *et al.*, 2007). Both of these ganglion cell types receive strong feedforward input from many cones. Direct recordings in cones have shown that their response amplitudes adapt to half of their maximal value on a background of ~4500 absorbed photons per second (Angueyra & Rieke, 2013). Despite this, midget and parasol ganglion cell responses begin to adapt at significantly lower light levels (Dunn *et al.*, 2007). Thus, adaption occurs when cones are not adapting and therefore must originate within the circuitry at lower light levels.

The task of controlling signal gain at the level of the retinal output is thought to be delegated to different circuit elements based on the reliability of their signals at different points

within the circuit operating range (Dunn *et al.*, 2007). Such a configuration allows labor to be divided amongst circuit components in a manner that optimizes performance. At very dim light levels, individual cone signals are not reliable enough to guide adaptation. Therefore, cones themselves do not adapt. Because downstream cells integrate signals from multiple cones, they benefit from a lower noise readout of the current input statistics. This allows them to adapt at lower light levels. As light levels increase, this mechanism saturates. By this point, individual cone signals have become reliable enough to guide adaptation, and cones begin to adapt.

A model in which adaptation is divided between cones and circuit-level mechanisms makes specific predictions about the retinal output, and ultimately perception. One example that has not been directly tested is whether adaptation is cone type specific. Does adaptation in the gain of signals originating in one cone type impact the gain of signals from another cone type? Cone signals are mixed at the first retinal synapse, thus if adaptation was occurring within the retinal circuitry, it would be predicted that adaptation produced by signals from one cone type would affect signals from another cone type. If adaptation was occurring within individual cones, it would be predicted that changes would be restricted to signals originating in these individual cones. In the case of primate midget and parasol ganglion cells, it would be predicted that under dim lighting conditions, where circuit adaptation dominates, adaptation due to signals from one cone type would have a similar effect on signals from other cone types. If light levels increased to the point at which individual cones were adapting, different cones would adapt independently of each other, both across types and spatially. Characterizing the conditions under which cone signals adapt independently or together serves as a direct test of the model that parasol and midget ganglion cell adaptation occurs through different mechanisms under different input conditions. This division of labor is perceptually relevant because whether or not cone types adapt together or separately will

determine how signals of one wavelength influence those of another. Evaluating cone type-specific adaptation in primate retina, as a first step in extending the work of Dunn et al., 2007, will be the topic of Chapter 4.

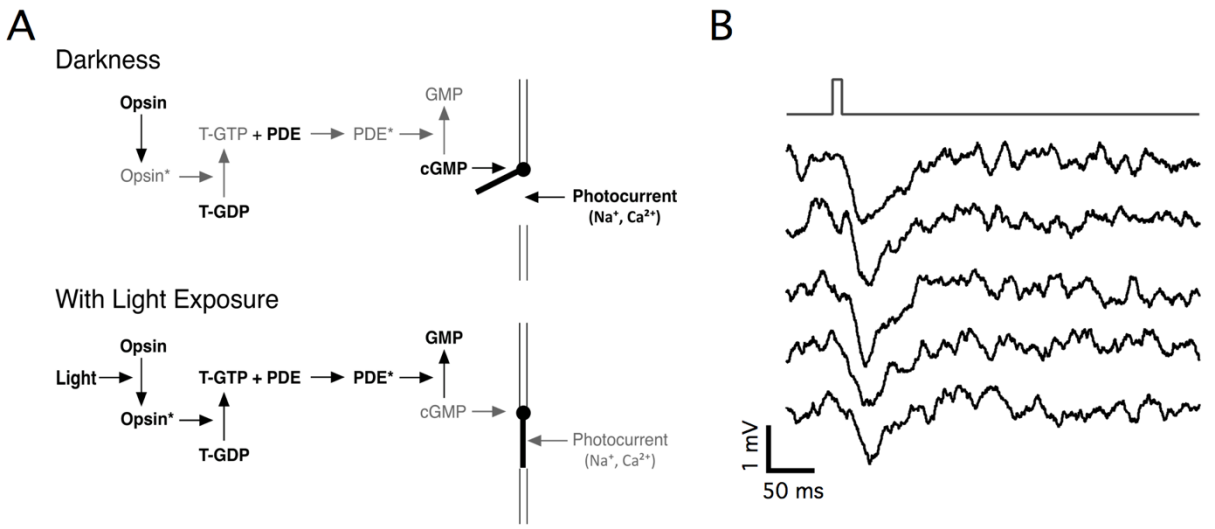

Figure 1.1. Signal detection by photoreceptors

(A) Phototransduction cascade in primate rod and cone photoreceptors. In darkness, a continuous dark current flows into the photoreceptor outer segments through cGMP-gated cation channels. With light exposure, photon absorption isomerizes opsin molecules, which activate the G protein transducin (T). Transducin activates phosphodiesterases (PDE), which break down cGMP, leading to channel closure and a reduction in the dark current.

(B) Example primate cone voltage responses following light absorption. Each traces is an individual response to a brief 10 ms flash causing approximately 150 absorbed photons. Flashes were delivered on a background of approximately 5,000 absorbed photons per second.

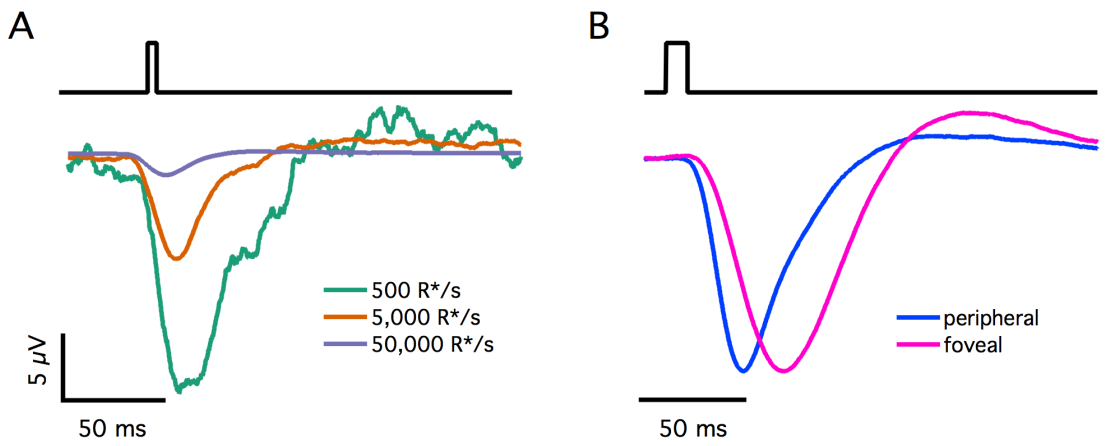

Figure 1.2. Primate cone flash responses

(A) Estimated average single photon responses in a primate L cone on backgrounds of 500, 5,000, and 50,000 R*/s. Single photon responses were estimated from responses to dim, 10 ms flashes by dividing the average response by the expected number of photon absorptions produced by each flash.

(B) Normalized, average responses of peripheral and foveal L and M cones to a dim 10 ms flash delivered on a background of 5,000 R*/s.

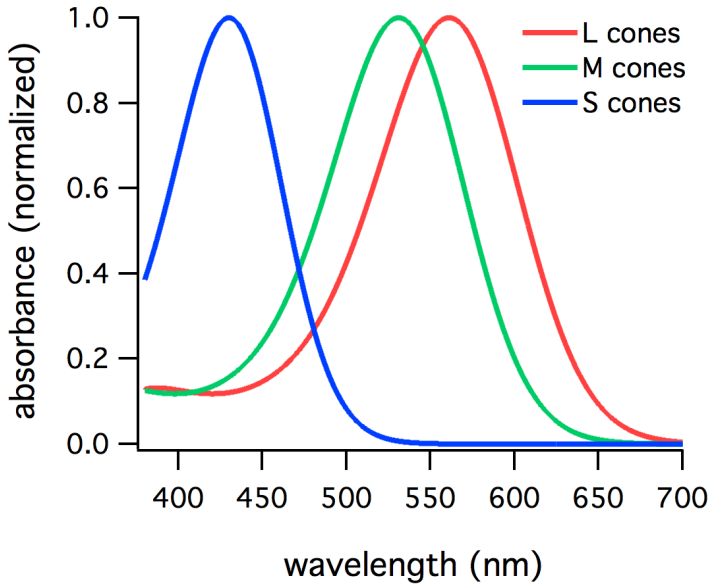

Figure 1.3. Cone spectral sensitivities

Normalized absorption spectra for primate cone opsins in the three classes of cone photoreceptors, providing them with their unique spectral sensitivities (from Baylor et al., 1987). Wavelengths of peak sensitivity are 430 nm, 531 nm, and 561 nm for S, M, and L cones, respectively.

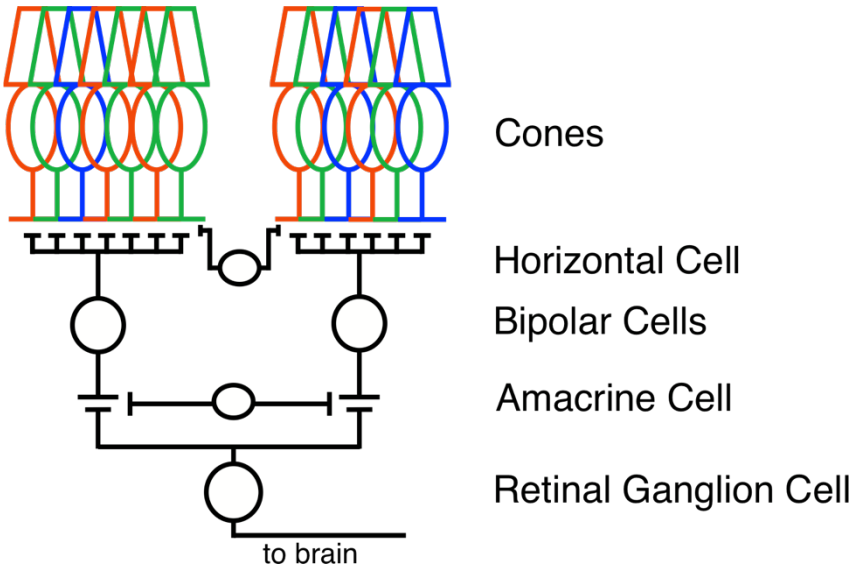

Figure 1.4. Canonical retinal circuitry carrying cone photoreceptor signals

Cone photoreceptors generate signals following photon absorption which they transmit to bipolar cells. Bipolar cells form synapses onto retinal ganglion cells, which send their axons to the brain. Lateral interactions shaping these feedforward signals are mediated by horizontal cells at the level of the cone to bipolar cell synapses, and by amacrine cells at the level of the bipolar cell to retinal ganglion cell synapses.

Chapter 2. PRIMATE S CONES ARE FUNCTIONALLY DISTINCT FROM L AND M CONES

2.1 ABSTRACT

Daylight vision starts with signals in three classes of cone photoreceptors sensitive to short (S), middle (M), and long (L) wavelengths. Models for cone vision often assume that that these three cone types are identical aside from differences in their spectral sensitivity. Psychophysical studies, however, show that perceptual sensitivity to rapidly varying inputs is lower for signals originating in S cones versus L and M cones. To determine if the cones themselves could contribute to such perceptual phenomena, we made intracellular recordings from primate S, M, and L cones to compare their light responses. We found that S cones generate slower light responses than L and M cones, show much smaller changes in response kinetics as mean light levels increase, and are noisier than L and M cones. These results compel the reevaluation of models for human visual perception that assume cones are homogenous across type.

2.2 INTRODUCTION

Sensory receptors pose fundamental limits to perception. Perceptual sensitivity to flickering lights, for example, is dramatically different at low and high light levels, and much of this dependence can be traced to differences in the kinetics of responses of the rod and cone photoreceptors themselves. Perceptual sensitivity to flickering lights is also lower for signals originating in short (S) wavelength cones than for signals originating in middle (M) or long (L) wavelength cones (Brindley *et al.*, 1966; Green, 1969; Smithson & Mollon, 2004; Lee *et al.*, 2009). Responses mediated by S vs L and M cones (hereafter LM cones) in post-retinal visual areas differ similarly

(Cottaris & De Valois, 1998; Tailby *et al.*, 2008). It is not known whether these differences originate in the cones themselves or the circuits reading out the cone signals.

Models for human cone vision often start with the assumption that signaling is identical across cone types apart from differences in wavelength sensitivity. Evidence for this assumption is limited by the small number of recordings from primate S cones (Baylor *et al.*, 1987; Schnapf *et al.*, 1990; Hornstein *et al.*, 2004; Cao *et al.*, 2014). Several considerations suggest that signaling could differ in S vs LM cones. First, responses of salamander and goldfish S cones are considerably slower than those of L cones (Rieke & Baylor, 2000; Howlett *et al.*, 2017), and salamander S cones exhibit lower noise (Rieke & Baylor, 2000). Second, the kinetics of responses of primate cones differ across retinal regions, providing a precedent for non-homogeneity of primate cones (Sinha *et al.*, 2017). Third, the evolutionary split between S cones and LM cones is estimated to have occurred more than 500 million years ago (Nathans *et al.*, 1986), providing ample opportunity for differences in signaling to emerge.

Here we directly test the hypothesis that S cones are identical to LM cones in their response kinetics, sensitivity to background light levels, and noise properties. By learning to identify S cones, we mitigated the challenges associated with their relative scarcity and collected a set of S cone recordings many times larger than those previously used to analyze their response properties. These data revealed that S cones differ from LM cones in kinetics, adaptation and noise. We show further that the differences in cone signaling impacts retinal output signals and makes specific predictions about how perceptual performance might differ from that based on the assumption of homogenous cone signaling.

2.3 RESULTS

The results below are divided into four sections: (1) comparison of the response kinetics of S and LM cones; (2) characterization of how the kinetics of S and LM cone responses depend on mean light level; (3) comparison of S and LM cone responses in retinal ganglion cells; and (4) comparison of noise in S and LM cones.

2.3.1 *S cone responses are slower than those of L and M cones*

Peripheral cones

To compare the kinetics of cone responses across spectral types, we recorded voltage responses to brief flashes delivered on background light levels giving matched photon absorption rates (R*/s) in each cone type. A cell's flash response was taken to be the average response across many such trials. Figures 2.1A and 2.1B show average responses across many cones in peripheral retina at two background light levels (5,000 R*/s and 50,000 R*/s, respectively). S cones had distinctly slower responses than L and M cones, and the L and M cone responses were near-identical.

Light responses can vary across different pieces of retina, potentially affecting cone kinetics measurements. To control for such variability, we compared the average time to peak of S cones with that of pooled LM cones from each piece of retina from which we recorded (Figures 2.1C,D). S cone responses were distinctly slower than LM cone responses across many retinas, and these differences are not explained by variability across preparations. Differences similarly persisted when we compared S cone responses to LM cone responses measured immediately before or afterwards in the same piece of retina (not shown).

We used the same procedure to compare L and M cone responses and check the validity of grouping them as a comparison point for S cone kinetics. When we compared the average L cone time to peak to the average M cone time to peak in each retina, the pairs clustered close to unity

(Figure 2.2). At 5,000 R*/s there was no measurable difference in the paired average M and L cone times to peak (-2.0 to +2.2 ms, 95% CI), while the difference in the paired average S cone and pooled LM cone times to peak was 8.5 ms (6.4 to 10.6 ms, 95% CI). At 50,000 R*/s these differences were 1 ms (-2.0 to +4.2 ms, 95% CI) and 11.5 ms (9.3 to 13.7 ms, 95% CI). Thus, L and M cone response kinetics differ minimally whereas S cone responses are substantially slower than LM cones at these light levels.

Foveal cones

L and M cone responses are slower in the fovea than the periphery (Sinha *et al.*, 2017). To determine whether S cones exhibit similar regional differences in kinetics, we compared responses of S cones in foveal (within 500 μm of foveal pit) and peripheral (>5,000 μm from foveal pit) retina. Similar to foveal LM cones, responses of foveal S cones were much slower than those of their peripheral counterparts across background light levels (2.1E,F).

Slower kinetics of foveal S cones relative to peripheral S cones do not mandate that foveal S cones will be slower than foveal LM cones. Because of the fovea's importance in perception, we also directly compared foveal S cone responses with those of foveal LM cones to determine if the differences in kinetics observed in peripheral retina held in the fovea. As above, we compared the average S cone and LM cone kinetics in each fovea we recorded from (Figures 2.1C,D). These data demonstrate that the slower kinetics of S cone responses relative to LM cone responses persist in the fovea.

S vs LM cone kinetic differences hold for periodic stimuli

To test the generality of the differences in cone kinetics seen in flash responses, we measured responses to additional stimuli. Many psychophysical studies probing kinetics of S cone mediated visual signals have used periodic stimuli (Brindley *et al.*, 1966; Marks & Bornstein, 1973;

Stockman *et al.*, 1991, 1993). Hence, we measured frequency tuning curves in current clamp for cones of each spectral type (Figures 2.1G,H). These curves quantify how robustly a given cone type responded to sinusoidal stimuli across a range of frequencies. As expected from the flash response data, the average S cone tuning curve shows weaker responses to high frequency modulations compared to LM cones. To quantify these differences, we calculated the frequency at which each cone's tuning curve dropped by a factor of ten from its maximum value (Figures 2.1G,H, insets). This frequency was substantially lower for S cone responses compared to LM cone responses. These results reaffirm the slower S cone kinetics observed in responses to brief flashes.

S vs LM cone kinetic differences originate in phototransduction

The kinetic differences between cone types described above could originate in phototransduction or in the conversion of transduction currents to inner segment voltages. A persistence of kinetic differences in voltage clamp would indicate an origin in phototransduction, as is the case in salamander cones (Rieke and Baylor, 2000). Restriction of kinetics differences to current clamp would indicate an origin in the current-to-voltage transformation, consistent with goldfish cones (Howlett *et al.*, 2017) and with the role of HCN channel activity in speeding photoreceptor responses (Barrow & Wu, 2009; Santina *et al.*, 2012).

To distinguish between these possibilities, we recorded voltage clamp responses to Gaussian noise stimuli. For each cell, we calculated the linear filter that optimally mapped from the stimuli to the cone's responses (Rieke *et al.*, 1997). Each cell's linear filter provides an estimate of its impulse response (i.e., its response to a very brief flash of light). Comparing the times to peak of these linear filters, we found that S cone current responses were slower than those of LM

cones from the same pieces of retina, consistent with a difference in phototransduction kinetics across cone types (Figure 2.3).

The results described thus far indicate that primate S cones have slower responses than LM cones across a range of experimental protocols and retinal regions. These kinetic differences persist in voltage clamp, indicating that they originate from differences in phototransduction.

2.3.2 *Adaptation of cone response kinetics differs between S cones and LM cones*

Cone photoreceptors operate over orders of magnitude of light intensity. Across this range, the kinetics of L and M cone flash responses change as they adapt to changing inputs (Dunn *et al.*, 2007; Angueyra & Rieke, 2013). To compare this process across cone types and evaluate how it impacts the difference between LM cone and S cone responses, we compared light responses across a range of mean light levels. The time to peak of S cone responses varied minimally across background light levels (Figure 2.4A). Across the same range of backgrounds, LM cone responses accelerated substantially as the background light level increased (Figures 2.4B, C). To control for cell to cell variability, we normalized each cone's times to peak such that the time to peak at 5,000 R*/s was 1. As mean light levels varied, these normalized response times to peak show little or no change for S cone responses and a robust change for LM cone responses (Figures 2.4D-F). Despite these differences in adaptation of response kinetics, we saw no appreciable difference across cone types in the adaptation of their response amplitudes (Figure 2.5).

We also compared responses kinetics by measuring temporal frequency tuning curves at 5,000 R*/s and 50,000 R*/s for each cone type (Figures 2.4G-I). As expected based on the flash response data, the frequency at which sensitivity fell ten-fold changed minimally in S cones between 5,000 R*/s and 50,000 R*/s (-3.68 to +2.23 Hz, 95% CI). In both L and M cones, there

was a significant increase in this frequency at 50,000 R*/s compared to 5,000 R*/s (3.44 to 11.89 Hz in M cones, 95% CI; 1.68 to 11.49 Hz in L cones, 95% CI).

Across multiple stimuli, S cone kinetics vary minimally with background light level. The constancy of their kinetics compared to LM cone kinetics provides a useful difference in signaling properties that can be used to test for contributions of different cone types to downstream cells and perception (see below and Discussion).

2.3.3 *Differences in cone response properties shape the retinal output*

Are the differences in the kinetics and adaptation of S cone signals maintained throughout retinal circuits and hence could they contribute to visual perception? To answer this question, we compared S- and LM-mediated responses of retinal ganglion cells. Cone signals traversing identical circuitry should be slower if they originate in S cones versus LM cones. Directly testing this prediction is difficult due to a lack of efficiently targetable ganglion cells receiving S and LM cone signals via identical pathways from each cone type to the ganglion cells. Thus, comparisons in ganglion cells are confounded by the potential for different kinetic changes introduced within separate pathways. To mitigate this, we tested the effect of cone properties on shaping ganglion cell responses by relying on the greater sensitivity of the kinetics of LM cones vs S cones to changes in mean light level (Figure 2.4). If differences in cone response kinetics are indeed propagated through the retinal circuitry, the difference between the kinetics of S vs LM cone responses should increase with increasing background, just as the cone responses themselves do.

Small bistratified retinal ganglion cells (SBCs) receive both S-ON input and LM-OFF input (Dacey & Lee 1994; Field et al. 2007). SBCs stratify in the inner plexiform layer and receive S cone input via S-ON bipolar cells (Figure 2.6A, Dacey & Lee 1994; Calkins et al. 1998). They receive opposite polarity L and M cone input from either or both of two pathways: (1) via an LM-

OFF bipolar cell receiving direct LM cone input; or (2) via the S-ON bipolar cell which receives LM input that reaches S cones through the H2 horizontal cell (Field *et al.*, 2007; Crook *et al.*, 2009; Packer *et al.*, 2010). These differences in the route that S and LM cone signals take to reach the RGC precluded comparing the absolute kinetics of their S-ON and LM-OFF responses. Nonetheless, if cone kinetics are influencing retinal output, we would predict that the kinetics of the S-ON response in SBCs would change significantly less across light levels than the kinetics of the LM-OFF response. To test this, we compared changes in the kinetics of the S-ON versus LM-OFF responses.

We recorded SBC spike responses to S cone or LM cone-isolating Gaussian noise stimuli (Figures 2.6B, C; see methods for stimulus construction). From these data, we constructed a linear-nonlinear model (LN model) consisting of the combination of a linear filter and a static nonlinearity that best describe the mapping from stimuli to spikes. The linear filter in this model captures the response kinetics while the static nonlinearity accounts for a nonlinear dependence of the response on the stimulus. The kinetics of the SBC responses were quantified as the times to peak of the linear filters (see Methods).

As shown in the right-hand panels of Figures 2.6B and 2.6C, the linear filters computed for S cone isolating and LM cone isolating stimuli exhibit the expected polarity for a cell generating S-ON and LM-OFF responses. The kinetics of the responses change between a background of 1,000 R*/s and 10,000 R*/s for both S-ON and LM-OFF stimuli. For each cell, we calculated the time to peak shift between 1,000 R*/s and 10,000 R*/s for the linear filters from both the S-isolating and LM-isolating stimuli (Figure 2.6D). In each recorded cell, the shift in time to peak of the S-cone mediated responses was smaller than that of the LM-cone mediated responses, as predicted from the cone data (Figure 2.6D). Furthermore, across the population, the average time

to peak shift for S-cone mediated responses was significantly less than that for LM-cone mediated responses. The average shifts seen in the population of SBCs agreed well with the average shifts seen in the cones themselves (Figure 2.6D). Thus, the differences in kinetics of cone responses shape retinal output signals.

2.3.4 *Noise in S cones is unique from that in LM cones*

Signal and noise together determine what information cones transmit to downstream circuitry and what limitations they impose on visual perception. Noise arises at multiple stages in the biochemical cascade of phototransduction (Schneeweis & Schnapf, 1999; Angueyra & Rieke, 2013). One source is thermal activation of the photoreceptor photopigment, and pigment thermal stability has been shown to depend on the wavelength of peak sensitivity (Barlow, 1957; Luo *et al.*, 2011). This hypothesis predicts that photoreceptors sensitive to longer wavelengths will be noisier, and this is the case in salamander cones (Rieke & Baylor, 2000). Noise in primate cones appears to originate primarily from sources other than photopigment thermal activation. Thus, it is unclear how noise will vary across cone types (Schneeweis & Schnapf, 1999; Angueyra & Rieke, 2013).

We recorded cellular noise across a range of background light levels in S, M, and L cones (Figures 2.7A, B, see methods and Angueyra and Rieke, 2013) and compared the measured noise to dim flash responses at each background (Figure 2.7C). Noise extended to frequencies far higher than the flash response spectrum (Figure 2.7C, Angueyra & Rieke 2013). Hence, we summarized our noise measurements by integrating noise across two frequency ranges – one that overlaps with the flash response and one that does not. We refer to these as the flash response range and high frequency range (Figure 2.7C).

As previously seen in salamander and primate LM cones, noise changes as a function of background light level (Figure 2.7A). Previous measurements from primate LM cones showed that as light levels increased from darkness, noise in the flash response range increased ~2-fold and then fell sharply (Angueyra & Rieke, 2013). This was attributed to the background light level introducing Poisson noise in photon absorption while being too dim to engage adaptation. At higher backgrounds, response adaptation appeared to outweigh increased noise in photon absorption, leading to decreased noise in the flash response range. We found that L, M and S cones all followed this behavior, but the increase in noise in S cones was significantly smaller than that in LM cones at 500 R*/s (Figure 2.7D). Such a difference could arise if the S cone flash response and hence Poisson fluctuations were smaller relative to noise when compared to LM cones. If this were the main source of differences in the noise properties across cone types, two predictions can be made: (1) adaptation of S cone noise in the high frequency range, where noise in photon absorption should have little effect, would be expected to be similar to that in LM cones; and (2) the number of isomerizations required to match the noise power would be expected to be higher in S cones at these backgrounds. Both predictions held true. Noise in terms of effective isomerizations is significantly higher in S cones at 0 and 500 R*/s (Figure 2.8).

The increased noise magnitude relative to the flash response in S cones at 0 and 500 R*/s suggests that detection thresholds may also be higher in S cones. While detection thresholds and noise effective isomerizations are closely linked, past work in LM cones has reported either or both of these values. To facilitate comparison to previous studies, we also calculated brief flash detection thresholds in each cone type. The detection threshold was defined as the flash response strength needed to match the noise power in a 200 ms integration window (Figure 2.7F). As

expected, S cone detection thresholds were higher than those of LM cones both in darkness and at 500 R*/s. Thresholds were similar across cone types at 5,000 and 50,000 R*/s.

The results described here show that S cone noise is higher than LM cone noise at dim light levels and comparable at higher light levels. This is contrary to predictions if noise was dominated by thermal activation of the photopigment and the thermal activation rate scaled with wavelength of peak sensitivity. The difference in cone noise is sufficiently large to impact cone detection thresholds and other perceptual tasks based on the cone signals (see Discussion).

2.4 DISCUSSION

Primate cones are often assumed to be functionally homogeneous across spectral types. Motivated by studies of cones across spectral types in other species (Rieke & Baylor, 2000; Howlett *et al.*, 2017) as well as recently reported differences in primate cones across eccentricity (Sinha *et al.*, 2017), we aimed to test this long-standing hypothesis. Our results demonstrate that S cone responses differ from those of LM cones in three ways. First, S cone responses are slower than LM cone responses in both peripheral and foveal retina. Second, the kinetics of S cone responses adapt minimally across background light levels, unlike responses of LM cones. Third, S cones have a lower signal to noise ratio at low mean light levels compared to LM cones, resulting in higher S cone flash detection thresholds. Finally, we show that the differences we see between cone types directly shape the output of the retina and are predicted to affect perception.

2.4.1 *Delay in S cone pathways begins at the first neuron of the visual system*

S cones produce slower flash responses and respond less robustly to high frequency sinusoidal stimuli than LM cones. The persistence of these differences in voltage clamp indicates that they originate in the phototransduction cascade and not the current-to-voltage transformation. These

differences likely contribute to our poorer perceptual sensitivity to rapidly modulated signals targeting S cones compared to signals targeting LM cones (Brindley *et al.*, 1966; Marks & Bornstein, 1973; Smithson & Mollon, 2004). Furthermore, the kinetics of S cone responses changed minimally with increasing mean light level, while responses of LM cones sped considerably. Perceptual experiments find a similar difference in the dependence of flicker fusion frequencies on mean light level for stimuli encoded by S vs LM cones (Brindley *et al.*, 1966; Marks & Bornstein, 1973).

The relevance of these differences across cones types is supported by the differences we found in the response kinetics of small bistratified ganglion cells. The kinetics of SBC responses to S cone isolating stimuli changed less with increasing mean light level than responses to LM cone isolating stimuli. Thus, differences in response kinetics across cone types are propagated through the retinal circuitry subserving SBCs. It remains to be seen whether these differences are preserved in the other parallel pathways carrying S cone signals. This approach also demonstrates that differences across cone types in the dependence of kinetics on background light level can be used to probe the contributions of different cone types to downstream circuitry and perception.

In addition to comparing S cones to LM cones, we directly compared a large dataset of L and M cones. Their responses were identical within the resolution of our measurements. Given that S cones diverged evolutionarily from the common ancestor of LM cones far earlier than L and M cones diverged from each other, it is not surprising that S cones differ more from LM cones than L and M cones differ from each other (Nathans *et al.*, 1986). Differences in photopigment stability, however, could cause L and M cones to differ in adaptational state and hence in kinetics. Our results tightly constrain any such differences.

2.4.2 *Noise differs across cone spectral types*

The origin of noise in cone photoreceptors differs between salamander and primate. Specifically, isomerization-like events in salamander L cones contribute significantly to their noise, while noise in primate LM cones is dominated by other sources (Schneeweis & Schnapf, 1999; Rieke & Baylor, 2000; Angueyra & Rieke, 2013). Salamander S cones have much lower noise, consistent with a more stable photopigment. Unlike the situation in salamander, primate S cones are noisier than LM cones at low background light levels. This results in higher flash detection thresholds for S vs LM cones.

2.4.3 *Implications of cone noise differences for color discrimination*

Human sensitivity to subtle changes in contrast, spatial structure and color is impressive. Noise in cone responses constrains sensitivity to these different stimuli because our perceptual resolution is limited to stimuli that elicit reliably distinct responses. How then does the elevated S cone noise relative to LM cone noise impact limits to perceptual sensitivity?

Humans can detect changes in wavelength of only a few nm compared to the ~100 nm width of the cone spectral sensitivity curves (Pokorny & Smith, 1970; Geisler, 1989; Zhaoping *et al.*, 2011). Discriminating between stimuli of different wavelengths relies on differences in relative cone activity levels. We used ideal observer models to evaluate the impact of cone noise on wavelength discrimination (see methods). We compared models with measured S cone noise with those in which noise in S cones was identical to that in M cones. Wavelength discrimination depends on how L, M, and S cone activation levels are chosen for each wavelength; hence we compared several approaches. In all cases, incorporating measured S cone noise decreased performance compared to predictions made assuming S cone noise was not elevated relative to

other cone types (Figure 2.9-2.12). These analyses demonstrate that the observed differences between S and LM cone noise are sufficiently large to impact perceptual sensitivity.

2.4.4 *Implications of cone differences in interpreting visual system function*

Considerable effort has gone into understanding retinal circuits due to their importance in explaining human vision as well as their experimental accessibility as neural circuits. Such work often aims to understand and ultimately model the transformation these circuits perform between light arrival and some measured response. These models attempt to assign different computations to different circuit elements. Cones perform a complex transformation on their inputs, thus making it difficult to differentiate between their role and that of downstream circuitry in implementing observed computations. Incorporating reliable cone response predictions into retinal models in an attempt to better define the inputs to downstream circuitry is an emerging approach. Only recently has it become possible to use validated models of the differences in LM cones across the visual field. Our results here expand upon this by providing the information necessary to construct models capturing differences between different spectral types of primate cones.

2.5 METHODS

2.5.1 *Tissue, cells, and solutions*

Electrophysiological recordings were performed on primate retina obtained through the Tissue Distribution Program of the University of Washington's Regional Primate Research Center. Recordings were made from retinas from *Macaca fascicularis, Macaca nemestrina,* and *Macaca mulatta* of both sexes, aged 2 through 20 years. All use of primate tissue was done in accordance with the University of Washington Institutional Animal Care and Use Committee. Tissue was obtained and prepared as described previously (Angueyra & Rieke, 2013; Sinha *et al.*, 2017). In

short, dark adapted (> 1 hour) retina stored in warm (32° C), oxygenated Ames medium was placed photoreceptor side up (cone recordings) or photoreceptor side down (retinal ganglion cell recordings) on a poly-lysine-coated coverslip (BD Biosciences) that served as the floor of our recording chamber. Throughout recordings, the tissue was continuously perfused with warm, oxygenated Ames solution.

2.5.2 *Patch-clamp recordings*

Cone patch clamp recordings were performed as described previously (Angueyra & Rieke, 2013; Sinha *et al.*, 2017). In short, we measured cone light responses using a combination of whole-cell voltage-clamp (holding potential = -60 mV) and current clamp (holding current = 0 pA) recordings. Extracellular recordings from retinal ganglion cells were performed as described previously (Sinha *et al.*, 2017). Data were low pass-filtered at 3 kHz, digitized at 10 kHz, and acquired using a Multiclamp 700B amplifier. All recordings were controlled using Symphony Data Acquisition Software, a piece of open-source, MATLAB-based electrophysiology software (https://github.com/symphony-das).

2.5.3 *S cone identification*

S cones make up a minority of the cone photoreceptors within the primate retina. While recording, the photoreceptor array was visualized using DIC microscopy, making all cones appear similar. Initially, we attempted to label S cones in *in vitro* retina using an antibody directed against the S opsin molecule (anti-OPN1SW, Santa Cruz Biotechnology, sc-14363). The labeling was noisy and weak, but this approach did allow us to encounter slightly more S cones than we would have by randomly selecting cones from the photoreceptor array. Due to the weak staining, the fact that the staining took a significant amount of time, and that we were unsure what effect the antibody

binding would have on the cell, we abandoned the staining procedure. Inspired by an approach discussed in Packer et al., 2010, we began attempting to target S cones based on their morphology and spacing within the photoreceptor array. We found that targeting cones that seemed to be slightly smaller, recessed, and out of place within the array formed by other photoreceptors dramatically increased the probability that the cones were S cones. Targeting cones in this manner allowed us to efficiently collect a large number of S cone recordings.

2.5.4 *Light stimulation*

Stimuli were presented from computer-driven LEDs with peak wavelengths of 406, 515, and 640 nm to provide the flexibility to effectively stimulate all 3 cone types. Light stimuli covered a ~500 μm disk centered on the targeted cell. All stimulus protocols were generated using custom-written MATLAB-based extensions of Symphony Data Acquisition Software, and delivered at 10 kHz. To calculate cone isomerization rates we used LED power measurements, measured LED spectra, primate photoreceptor spectra from Baylor et al., 1987, and an effective collecting area of 0.37 μm^2 (Schnapf et al. 1990).

Cone isolating stimuli were constructed using a matrix that mapped from LED input to our calculated isomerizations in each cone type. The inverse of this matrix maps from isomerizations in each cone type to an input to each LED. Using this matrix, we were able to specify our stimuli in terms of isomerizations to each cone type. It is notable that any failures in isolating S cones versus LM cones would have decreased the magnitude of any differences we saw in the analysis presented in Figure 2.6.

2.5.5 *Analysis*

All data were analyzed using custom-written MATLAB analysis routines.

Time to peak calculation: All time to peak analyses were repeated using a series of different techniques to calculate the times to peak of cone flash responses and small bistratified ganglion cell linear filters. Results remained significant regardless of which technique was used. For the first approach, we took the time at which the raw average response or linear filter reached its maximal value. Due to unavoidable noise, it was apparent in some recordings that a random spike in noise had affected the time to peak determination. To control for this, we used two fitting-based approaches. For the first, we fit a truncated Gaussian distribution spanning ~20 ms to the peak region of the average flash response or linear filter. The time to peak was taken to be the time at which the Gaussian fit reached its maximal value. The final approach involved fitting a function previously shown to capture the structure of the flash response (Equation 2.1). We found this function to have the representational power necessary to fit both cone flash responses and SBC linear filters and we defined the time to peak as the time at which this fit function reached its maximal value. For cones, all times to peak response reported here were calculated using the truncated Gaussian fitting technique. Small bistratified cell linear filter times to peaks were calculated using fits from Equation 2.1.

$$f(t) = \alpha \times \left[\frac{(\frac{t}{t_{rise}})^4}{1+(\frac{t}{t_{rise}})^4}\right] \times \left[e^{-\left(\frac{t}{t_{decay}}\right)}\right] \times \left[cos(\frac{2\pi t}{t_{osc}} + \phi)\right] \quad (2.1)$$

Spectral Analysis: Noise and flash response power spectra were calculated using MATLAB's built-in fast Fourier transform and converted to two-sided power spectral densities with units of pA^2/Hz. Dim flash response recordings contain a combination of cellular noise, instrumental noise, and the flash response. To isolate the flash response power, power spectral densities were computed using fits to the dim flash response (using Equation 2.1). To compute the power in different frequency ranges, the power spectral densities were integrated across the range.

Noise Isolation: Cellular noise isolation was performed as in Angueyra & Rieke 2013. Any current fluctuations in a voltage clamp recording are a combination of noise arising in phototransduction in the cones (cellular noise) and noise from the recording itself (instrumental noise). Providing a near-saturating light stimulus shuts down phototransduction and isolates instrumental noise. Under the assumption that cellular and instrumental noise are independent, cellular noise can be isolated by simply subtracting the power spectrum of the noise in saturating light from the noise power spectrum at each background.

Temporal Frequency Tuning Curves: Frequency tuning curves were constructed using a cone's responses to sinusoidal stimuli across a range of frequencies. To quantify a cone's response amplitude at a given frequency, the best fit was found using the following equation:

$$y = a * sin(2 * pi * fx + b) + c \qquad (2.2)$$

f was matched to the frequency of the stimulus. b and c were free to vary. The response amplitude was taken to be the fit value of a divided by the contrast of the stimulus. This contrast normalization step was necessary because higher contrasts were required to elicit responses at higher frequencies where the cells were less responsive. Before averaging tuning curves across cells, each cell's tuning curve was normalized such that its amplitude at the frequency with the strongest response was 1.

The frequency at which a cone's response decreased by a factor of 10 was calculated by interpolating a smooth function fit to its frequency response curve. Under an assumption of linearity, the shape of the frequency tuning curve is equivalent to the power spectrum of the cone flash response. Therefore, the best fit was found for each curve using the power spectrum of Equation 2.1. Best fits were found using the following loss function:

$$L(\theta) = \sum_i \left| log(\frac{F(\omega_i,\theta)}{D(\omega_i)}) \right| \qquad (2.3)$$

Where $F(\omega_i, \theta)$ is the prediction from a fit with parameters θ at the frequency ω_i and $D(\omega_i)$ is the data.

Adaptation Curves: For each cell, average dim flash responses across a range of background light levels were fit with Equation 2.1. The amplitude of such a response was taken to be the amplitude of the fit function and converted to a response per isomerization by dividing by the flash strength. A cell's response amplitudes per isomerization across background light levels were fit with a Weber curve:

$$\frac{\gamma_B}{\gamma_D} = \frac{1}{(1+\frac{I_B}{I_0})} \qquad (2.4)$$

The half max amplitude of the adaptation curve was taken to be the value of I_0 from the fit. Fits were performed using the loss function from Equation 2.3. Prior to averaging adaptation curves across cells, each was scaled such that its best fit to Equation 2.4 would have a response per isomerization of 1 on a background of 0 R*/s.

Cone Linear Filter Calculation: Linear filters were computed using cone responses to white noise stimuli as done previously (Wiener, 1949; Rieke *et al.*, 1997).

LN Model Construction: LN models were constructed from small bistratified ganglion cell responses to white noise stimuli through a series of steps. First, spike detection was performed. Then, the optimal linear filter mapping from the white noise stimuli to binary vectors of spike responses was computed as in Rieke et al., 1997. Finally, a nonlinearity was calculated to map the output of a stimulus convolved with this linear filter (generator signal) to a probability of spiking. This was constructed by convolving each white noise stimulus vector with the calculated linear filter and, based on the detected spikes, determining the probability of a spike given some generator signal. Nonlinearities were fit with Gaussian cumulative distribution functions.

2.5.6 *Modeling*

Ideal observer models were constructed in which the observer had access to the number of isomerization-like events in a patch of cone photoreceptors (Geisler, 1989). Isomerization-like events were taken to include both stimulus-induced isomerizations and an additional number of isomerizations whose power matched that of the intrinsic cellular noise (Figure 2.8). At any wavelength, the probability of a photon being absorbed in a given cone type was calculated using cone fundamentals from Stockman & Sharpe 2000 scaled such that they peaked at 1.0, 1.0, and 0.2 for L, M, and S cones, respectively (Zhaoping *et al.*, 2011). This scaling was intended to account for the wavelength dependence of the optics of the eye. The mean stimulus-induced isomerization count in a cone of type c (with fundamental $p_c(\lambda)$) to a stimulus of wavelength λ and intensity of I photons was calculated as:

$$r_{stim,c} = I * p_c(\lambda)$$

Our cone noise measurements allowed us to predict noise effective isomerization rates as a function of background light level. To make this prediction, we converted the absorbed photon count ($r_{stim,c}$) to an isomerization rate using an integration time of 200 ms. The overall rate of isomerization-like events, including contributions from intrinsic cellular noise, was calculated by interpolating the relationship we measured between mean background isomerization rates and effective noise isomerization rates for each cone type (Figure 2.8). This was converted back to an isomerization count within the integration window by multiplying the rate by the integration time.

In addition to making predictions based on our cone noise measurements in each cone type as described above, we considered three modified cases: (1) S cone noise was assumed to be equivalent to M cone noise and thus was predicted using M cone noise measurements, while L and M cone noise was still predicted using their respective noise measurements; (2) S cones were

omitted entirely from the ideal observer model; and (3) intrinsic noise in photoreceptors was omitted and cone noise was taken to be only the extrinsic noise resulting from fluctuations in photon absorption.

For each model, the ideal observer had access to the signals in 6 L cones, 3 M cones, and 1 S cone to approximate cone type ratios found in primate (as done in Zhaoping et al. 2011). Isomerization-like events in individual cones of each type were pooled to give a total number of isomerizations for each cone type, yielding a set of 3 values for each stimulus. Each point represents the predicted mean number of isomerization-like events in each cone type for the stimulus. The actual number of L, M, and S isomerization-like events will vary from trial to trial due to noise in both photon absorption and the phototransduction cascade. Assuming Poisson noise in the total number of isomerization-like events, noise around each point was described by a diagonal covariance matrix with the L, M and S components of the point serving as the variances of their respective dimensions. As the matrix is diagonal, covariance between signals in different cone types was assumed to be 0.

To calculate the discriminability of two points in this space, the Fisher Linear Discriminant was used (Duda *et al.*, 2001). Two points were considered discriminable when their discriminability index (d') was 1.

Discrimination thresholds were predicted using four approaches to calculate the LMS space point at each wavelength. They were: (1) using a constant stimulus intensity for which an equivalent number of photons were delivered, but not necessarily absorbed, to each cone for all wavelengths; (2) holding constant the L2 norm of the points in LMS space for each wavelength; (3) holding constant the sum of the L and M components of each LMS space point; and (4) holding constant the sum of the L, M , and S components of each LMS space point.

To calculate the discriminability threshold at some wavelength, λ_i, using the constant stimulus intensity approach (Figure 2.10), we first found the pooled number of isomerization-like events for each cone type in response to a stimulus at λ_i with some intensity, I. To find the number of isomerization-like events for a nearby wavelength, λ_j, we started by calculating the pooled number of stimulus-induced isomerizations for each cone type to a stimulus at λ_j with the same intensity I. This is equivalent to enforcing that the same number of photons were delivered to each cone at both λ_i and λ_j. Assuming that on the timescale of a wavelength discrimination task there would not be changes in the intrinsic noise, we calculated the final number of isomerization-like events for the stimulus at λ_j as the sum of the intrinsic noise calculated for λ_i and the total stimulus induced isomerizations at λ_j. The intrinsic cellular noise for λ_i was calculated as the difference between the isomerization-like event rate predicted from experimental data and the stimulus-induced isomerization rate. When discrimination was performed, the covariance matrix was assumed to be constant, and taken to be that of the point for λ_i.

LMS space is a 3 dimensional space where each dimension represents the number of isomerizations in a single L, M, or S cone. The cone responses for each wavelength fall on a line extending from the origin. The constant LMS norm (Figure 2.9), L + M + S plane (Figure 2.11) and L + M plane (Figure 2.12) cases all place a constraint on where in LMS space a stimulus of some wavelength must fall. For a constant LMS norm and some wavelength, λ_i, the intensity must be chosen such that $L^2 + M^2 + S^2 = c^2$ where c is the specified target LMS norm. To maintain a constant LMS norm at all wavelengths, the intensities of the stimuli were chosen at each wavelength to find the point satisfying the above relationship. This is equivalent to forcing all points to lie on a sphere in LMS space that has a radius of c. In the case of the L + M plane, the

intensity was chosen such that L + M = c. For the L + M + S plane, it was chosen such that L + M + S = c. In either case, c controlled the distance of the plane from the origin.

To calculate the discriminability threshold at some wavelength, λ_i, for the constant LMS norm, L + M plane, or L + M + S plane case, we first found the intensity of stimulus at, λ_i, that would fall on the specified plane or sphere in LMS space. From there, we calculated the pooled stimulus-induced isomerizations and effective isomerization-like events for that wavelength. The difference between those numbers was taken to be the contribution of intrinsic noise. To calculate the discriminability of some neighboring wavelength, λ_j, we found the stimulus intensity necessary for a stimulus of that wavelength to fall on the same specified plane or sphere in LMS space. We then found the pooled stimulus-induced isomerizations for a stimulus of that wavelength and intensity. For models including intrinsic noise, we reached a final effective isomerization-like event count for λ_j by adding the intrinsic noise from λ_i to the pooled stimulus-induced event count at λ_j. For the extrinsic noise only model the effective isomerization-like event count was taken to be the stimulus-induced isomerization count. To calculate discriminability, the covariance matrix for the LMS response was assumed to be constant, and taken to be that of the point for λ_i.

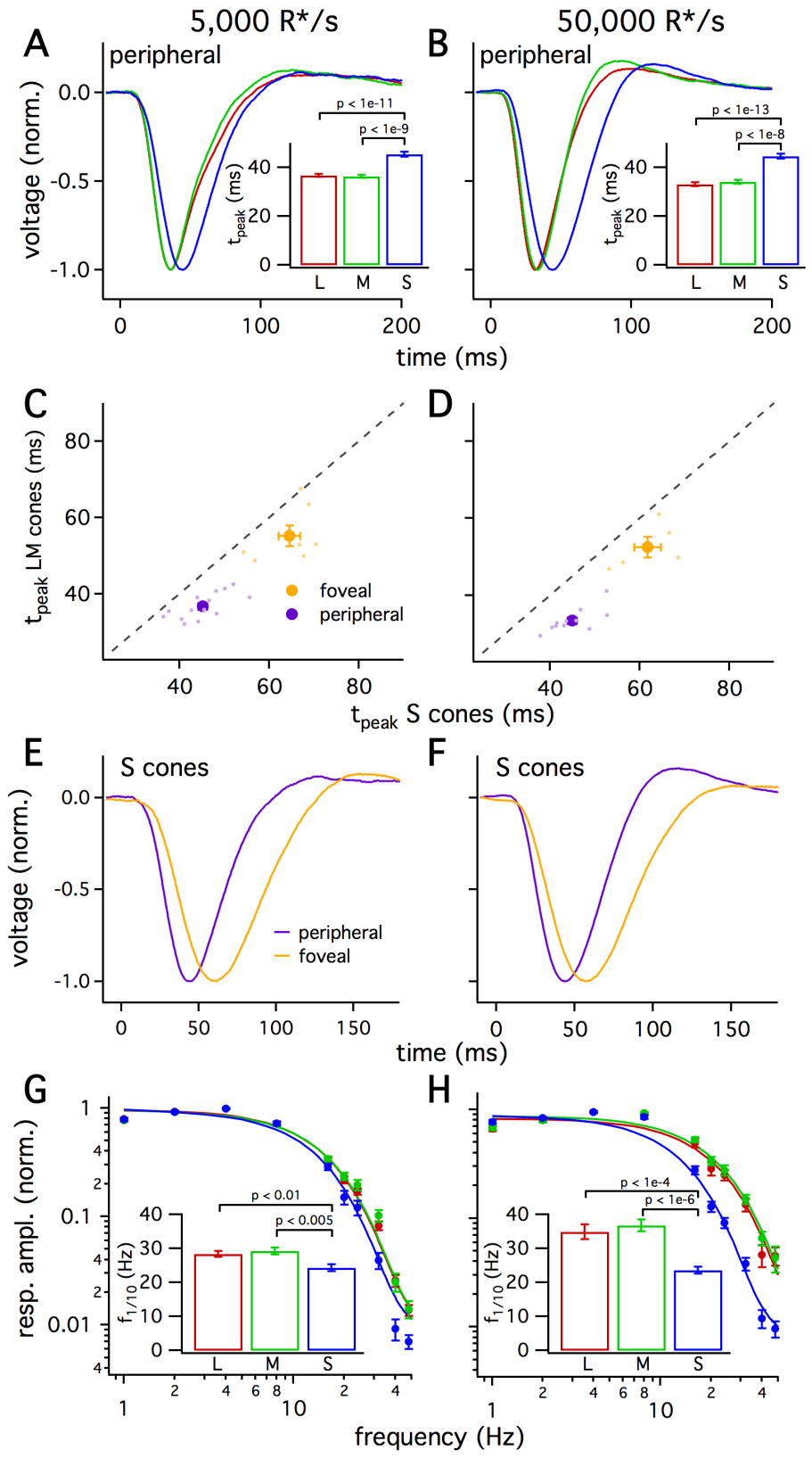

Figure 2.1. S cones are slower than L and M cones across retinal eccentricities

(A) Average normalized voltage responses of L, M and S cones on a background of 5,000 R*/s. Inset shows times to peak across cone types. The mean ± sem times to peak were 36.7 ± 0.6 ms for L cones (n = 49), 36.3 ± 0.6 ms for M cones (n = 26), and 45.3 ± 0.9 ms for S cones (n = 36). P values from unpaired t-test.

(B) As in Figure 2.1A for data collected on a background of 50,000 R*/s. The mean ± sem times to peak were 33.1 ± 0.7 ms for L cones (n = 42), 34.1 ± 0.9 ms for M cones (n = 17), and 44.5 ± 0.9 ms for S cones (n = 28).

(C) Average time to peak of S cones compared to average time to peak of pooled L and M cones in peripheral (purple) and foveal (gold) retina on a background of 5,000 R*/s. Each smaller point represents the average times to peak from a single piece of retina. Each large point with error bars represents the mean ± sem across all pieces at a given eccentricity. S cones are significantly slower than their LM counterparts in peripheral ($p < 10^{-6}$, paired t-test) and foveal ($p < 0.05$, paired t-test) retina. Average responses for Figure 2.1A were across all peripheral cells included in this analysis.

(D) As in Figure 2.1C except for data collected on a background of 50,000 R*/s. Average responses for Figure 2.1B were across all cells included in this analysis. Peripheral ($p < 10^{-6}$, paired t-test) and foveal ($p < 0.05$, paired t-test) S cones were significantly slower than their LM counterparts.

(E) Average S cone flash responses across population in peripheral and foveal cones on a background of 5,000 R*/s.

(F) As in (E) on a background of 50,000 R*/s.

(G) Frequency tuning curves across cone types. Points with error bars are mean ± sem temporal frequency sensitivities of L, M and S cones on a background of 5,000 R*/s. Values are the

normalized response amplitudes across frequencies. Curves show best fit of power spectrum of Equation 2.1 to population data. Inset shows mean ± sem frequencies at which response amplitudes decreased to 10% of their maximum value, which were 28.4 ± 0.9 Hz in L cones (n = 26), 29.2 ± 1.0 Hz in M cones (n = 17), and 24.4 ± 1.0 Hz in S cones (n = 15). P values from unpaired t-test.

(H) As in Figure 2.1E for data collected on a background of 50,000 R*/s. Mean ± sem temporal frequencies for 10% maximum gain were 35.0 ± 2.2 Hz in L cones (n = 17), 36.9 ± 1.8 Hz in M cones (n = 21), and 23.6 ± 1.0 Hz in S cones (n = 16).

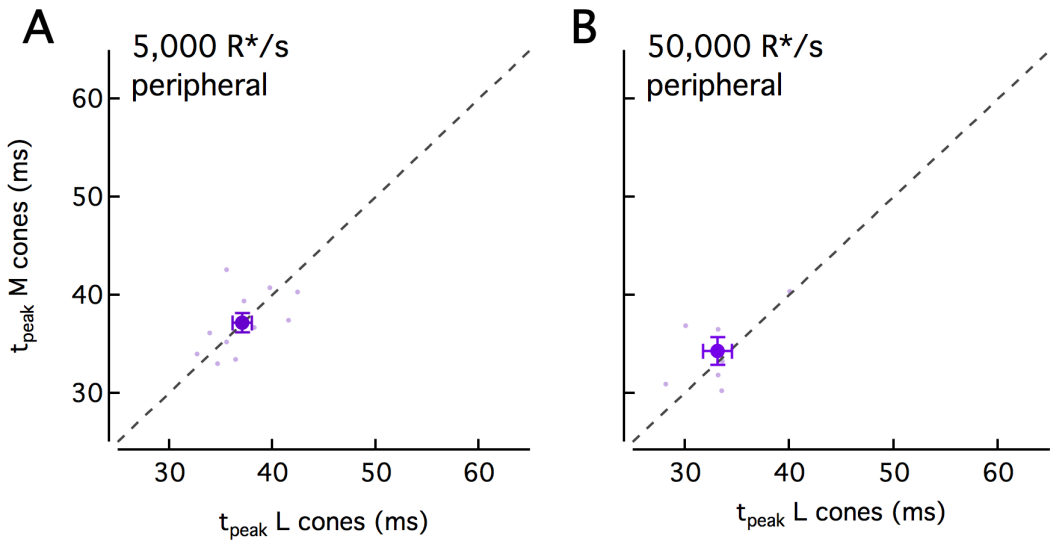

Figure 2.2. L and M cone response kinetics are similar

(A) Average time to peak of L cones compared to average time to peak of M cones in peripheral retina on a background of 5,000 R*/s. Each smaller point represents the average times to peak from a single piece of retina. Large point with error bars represents mean ± sem across all pieces. (B) As in panel A for data collected on a background of 50,000 R*/s.

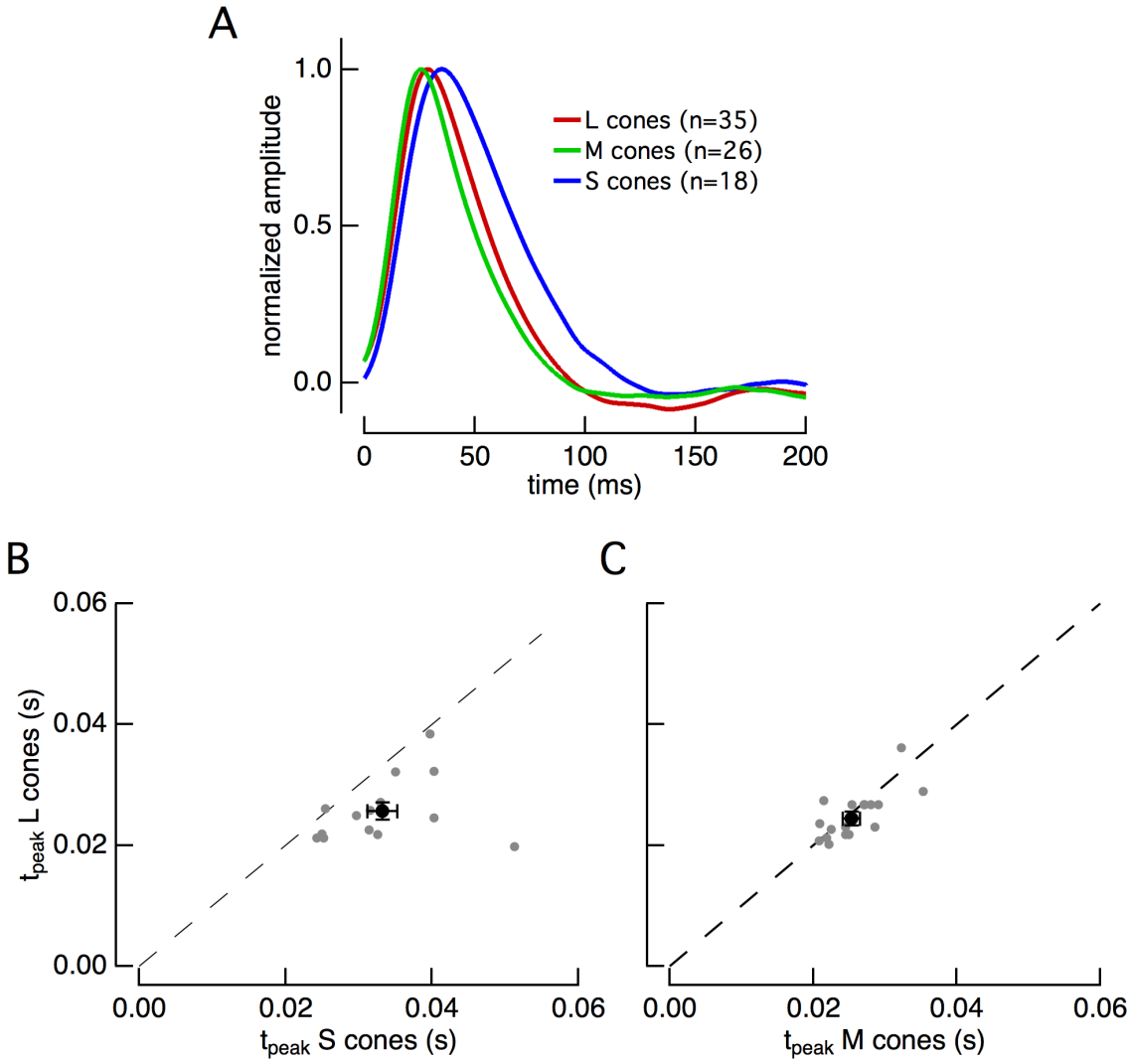

Figure 2.3. Cone kinetic differences remain in voltage clamp

(A) Average normalized linear filters of L, M and S cones on a background of 2,500 R*/s. Filters were calculated to be those that optimally map Gaussian noise stimuli to measured cone responses.

(B) Comparison of times to peak of S cone versus L cone linear filters. Each point represents the times to peak of filters from an S cone and an L cone from the same piece of retina. S cones times to peak were significantly shorter than M cones ($p < 0.005$, paired t-test).

(C) Comparison of times to peak of M cone versus L cone linear filters. Each point represents the times to peak of filters from an M cone and an L cone from the same piece of retina. L and M cone times to peak were not significantly different ($p > 0.05$, paired t-test).

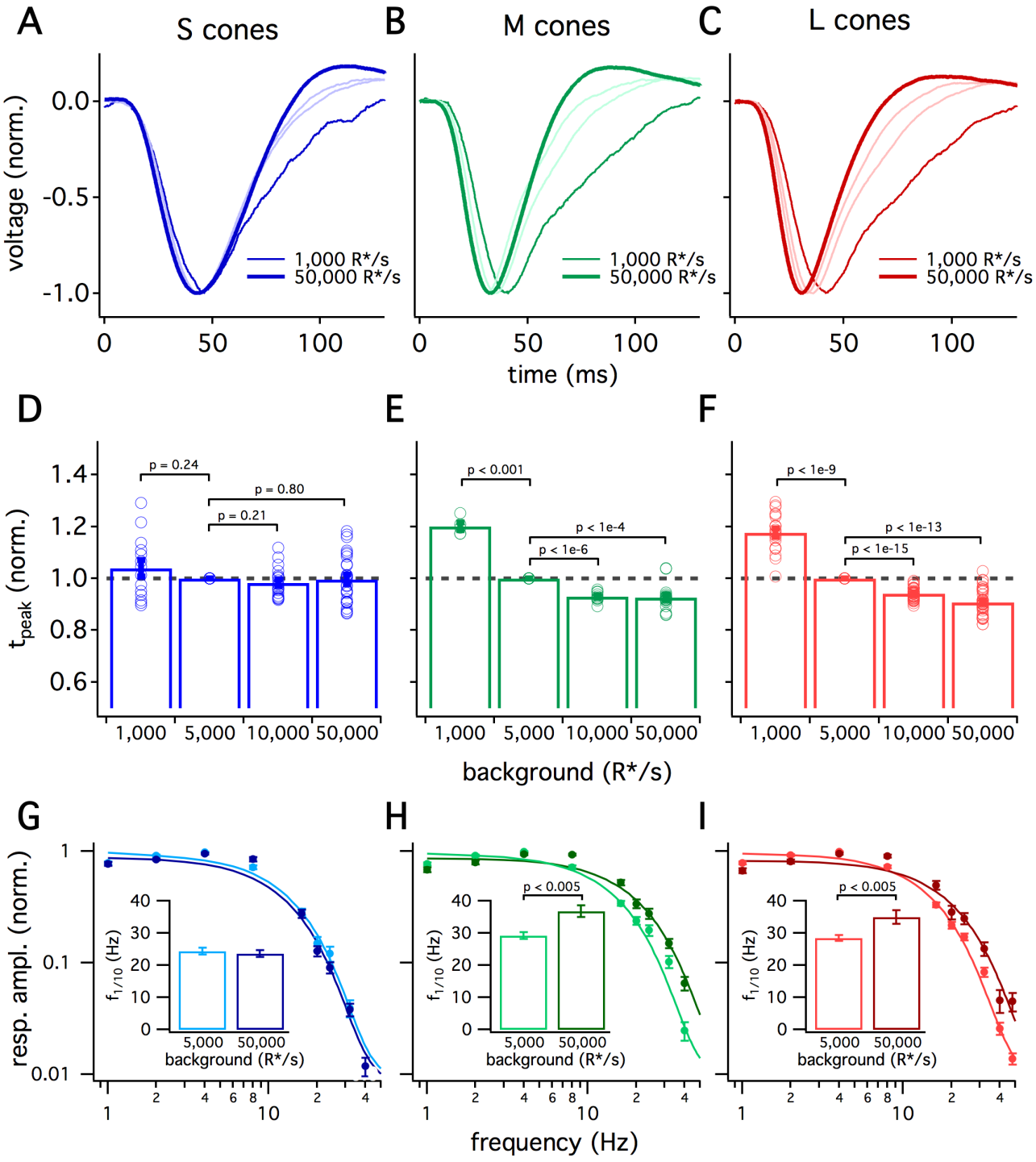

Figure 2.4. S cone kinetics change minimally across background light levels

(A-C) Average normalized voltage responses of S (A), M (B), and L (C) cones on backgrounds of 1,000 R*/s (thin line) and 50,000 R*/s (thick line). Lighter lines show responses at intermediate light levels of 5,000 R*/s and 10,000 R*/s.

(D-F) Mean ± sem relative times to peak across backgrounds in S (D), M (E), and L (F) cones. In each cell, the time to peak at each background was normalized by the time to peak at 5,000 R*/s in that cell. P values from one-sample t-test.

(G-I) Frequency tuning curves at 5,000 R*/s and 50,000 R*/s in S (G), M (H), and L (I) cones. Points with error bars are mean ± sem normalized response amplitudes across frequencies. Curves show fit of power spectrum of Equation 2.1 to population data. Inset shows mean ± sem frequencies at which response amplitudes decreased to 10% of their maximum value at either background. At 5,000 and 50,000 R*/s, these frequencies were 24.4 ± 1.0 Hz (n = 15) and 23.6 ± 1.0 Hz (n = 16) in S cones, 29.2 ± 1.0 Hz (n = 17) and 36.9 ± 1.8 Hz (n = 21) in M cones, and 28.4 ± 0.9 Hz (n = 26) and 35.0 ± 2.2 Hz (n = 17) in L cones. P values from unpaired t-test.

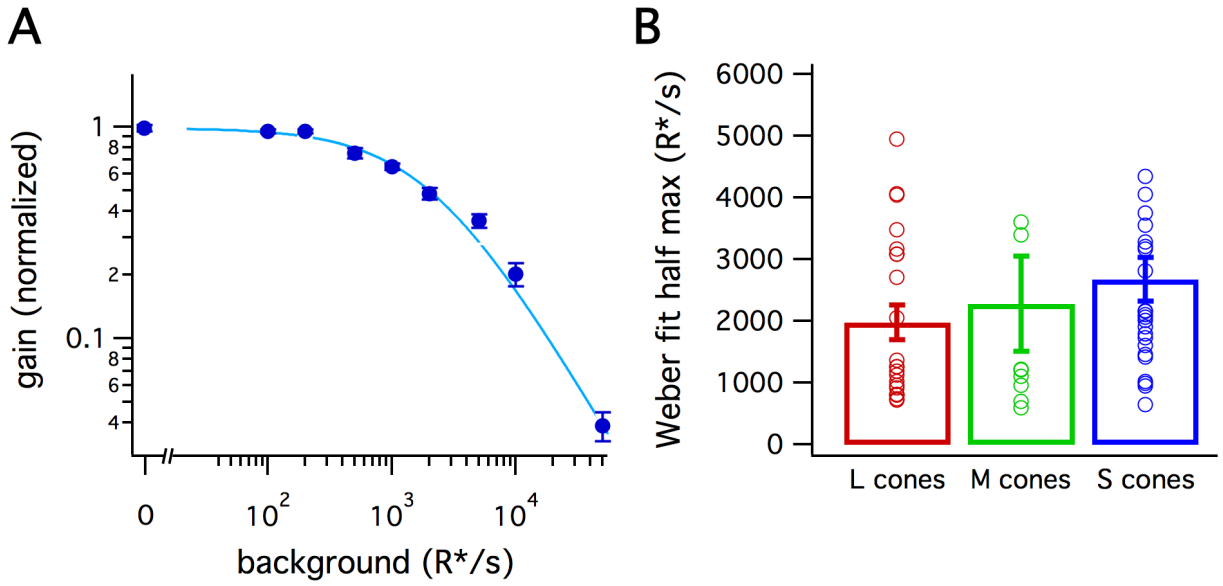

Figure 2.5. Response amplitude adaptation across cone types

(A) Response amplitude adaptation in S cones. Points with error bars represent mean ± sem normalized gains across backgrounds. Prior to averaging, values from each cell were fit to Equation 2.4 and scaled such that the gain of the fit on a background of 0 R*/s was 1. Solid line shows fit of Equation 2.4 to population data, demonstrating that S cone adaptation can be described by this equation.

(B) Half-max backgrounds from Weber curve (Equation 2.4) fits to amplitude adaptation data in each cone type. Error bars represent sem.

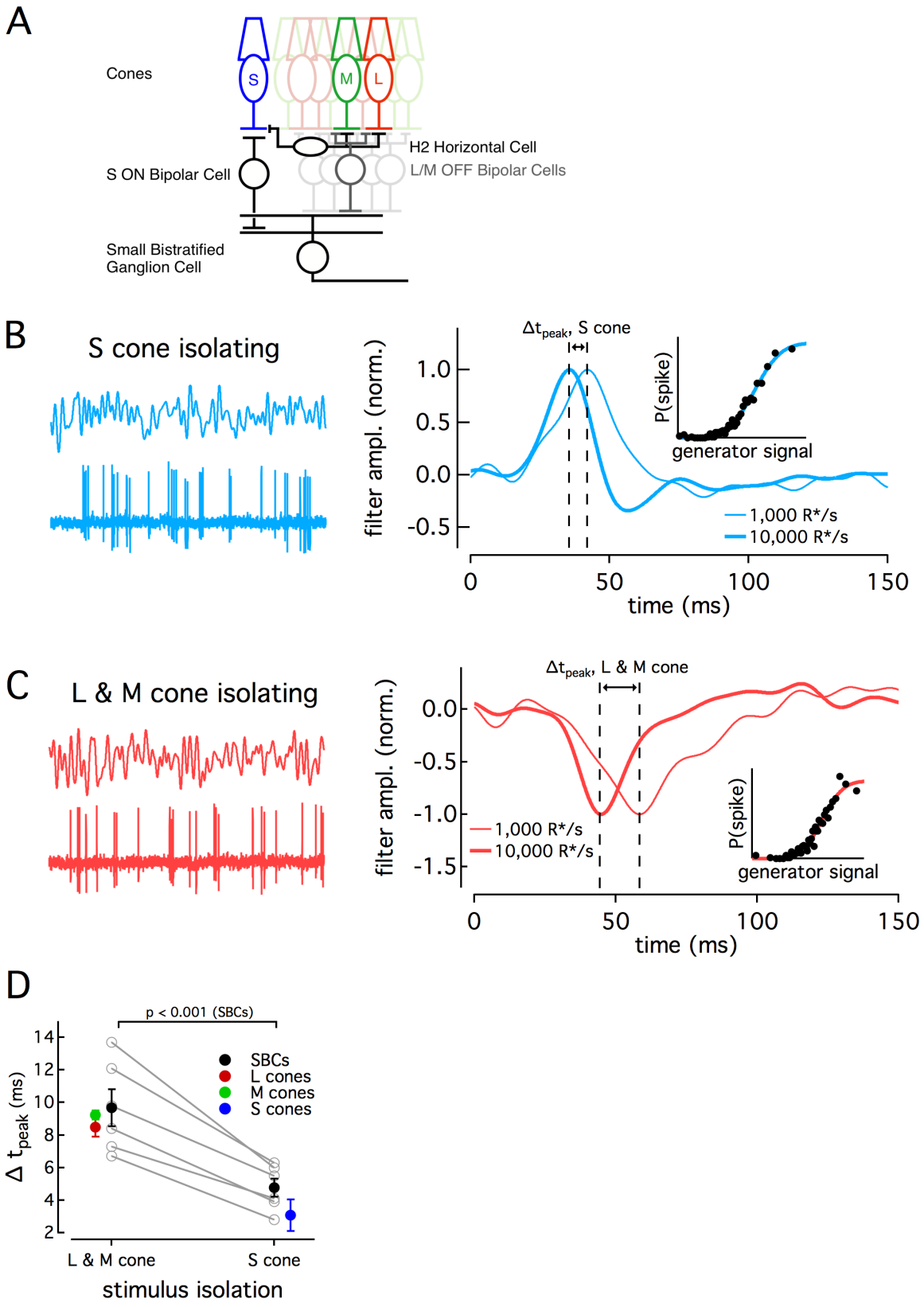

Figure 2.6. Differences in cone adaptation affect retinal ganglion cell responses

(A) Previously described circuitry upstream of SBCs. S-ON signals travel from S cones through S ON Bipolar Cells to SBCs. L/M-OFF signals travel from L and M cones through H2 horizontal cells to S cone terminals, where they are transmitted to SBCs via S ON Bipolar cells. Alternatively, L and M cone signals may be carried to SBCs directly via an L/M OFF Bipolar cell.

(B) Example response of SBC to S cone isolating white noise stimulus (left). Example Linear-nonlinear (LN) model derived from SBC responses to white noise stimuli (right). Normalized linear filters shown for backgrounds of 1,000 and 10,000 R*/s. Time to peak shifts between 1,000 R*/s and 10,000 R*s were taken to be the difference in the times to peak of the linear filters at each background. Inset shows nonlinearity mapping from generator signal to spiking probability.

(C) Example response and LN Model as in (C), but for L/M-OFF response.

(D) Comparison of time to peak shifts in S-ON and L/M-OFF SBC responses. Mean ± sem shifts were 9.7 ± 1.1 ms for L/M-OFF responses and 4.8 ± 0.7 ms for S-ON responses (n = 6). Shifts in each cone type between 1,000 and 10,000 R*/s are shown for comparison. Shifts were 3.1 ± 1.0 ms in S cones (n = 14), 9.2 ± 0.3 ms in M cones (n = 7), and 8.49 ± 0.6 ms in L cones (n = 22). P value from paired t-test.

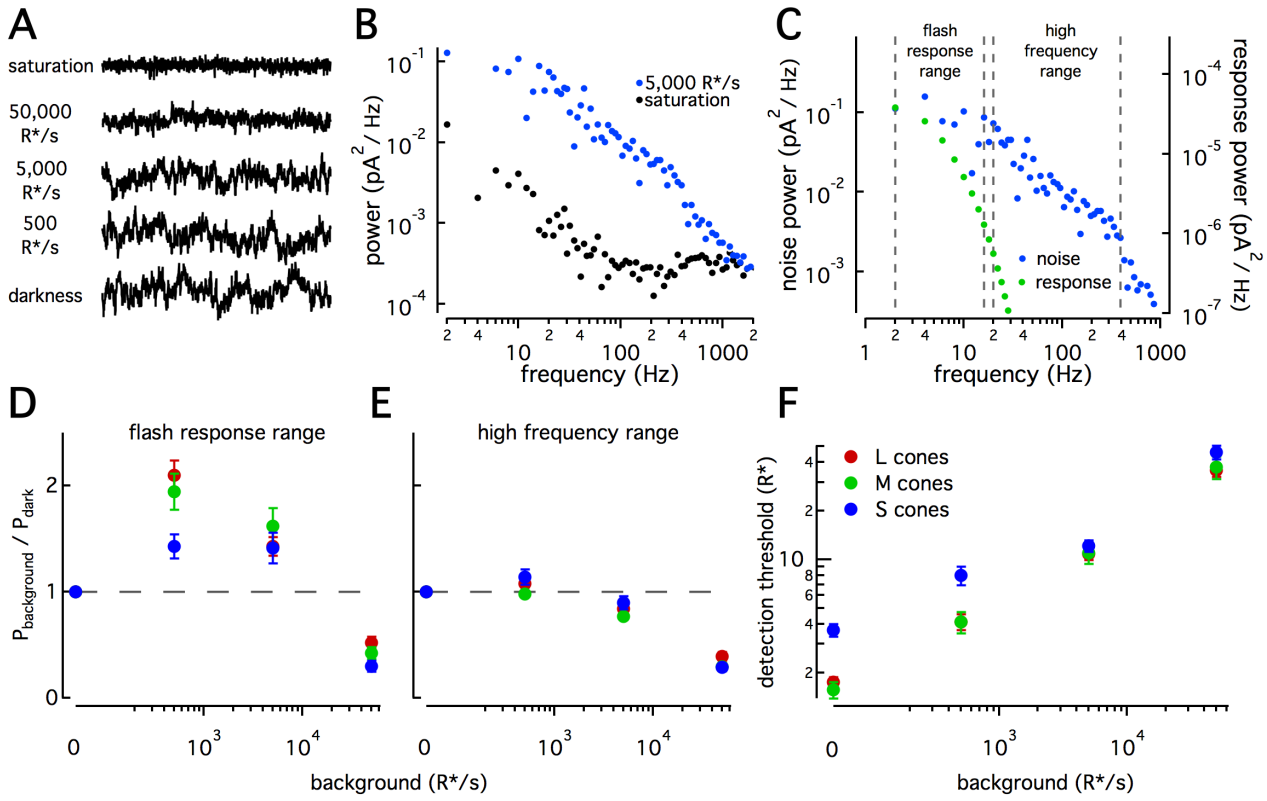

Figure 2.7. S cones are noisier under dim lighting conditions

(A) Example current responses from an S cone on backgrounds of 0, 500, 5,000, and 50,000 R*/s and in saturating light.

(B) Example power spectra of noise at 5,000 R*/s (blue) and in saturating light (black) from an S cone. Spectrum at 5,000 R*/s includes contributions from cellular as well as instrumental noise.

(C) Example isolated cellular noise spectrum (left axis, blue) and flash response spectrum (right axis, green), both on a background of 5,000 R*/s. Dashed vertical lines identify bounds for flash response and high frequency ranges used in (D-F).

(D) Noise power in flash response range. Values show mean ± sem powers across backgrounds normalized by the power in darkness. Dashed horizontal line shows noise power in darkness. The change in S cone noise at 500 R*/s was significantly lower than that in L and M cones (S vs M, $p < 0.05$; S vs L, $p < 0.001$; unpaired t-test).

(E) As in (D) but for noise in high frequency range.

(F) Detection thresholds across backgrounds in S (n = 9), M (n = 9) and L (n = 15) cones. Plotted values show mean ± sem. In darkness, mean ± sem threshold is 3.67 ± 0.33 R* in S cones, 1.57 ± 0.18 R* in M cones, and 1.75 ± 0.12 R* in L cones. At 500 R*/s it is 7.95 ± 1.02 R* in S cones, 4.13 ± 0.63 R* in M cones, and 4.12 ± 0.46 R* in L cones.

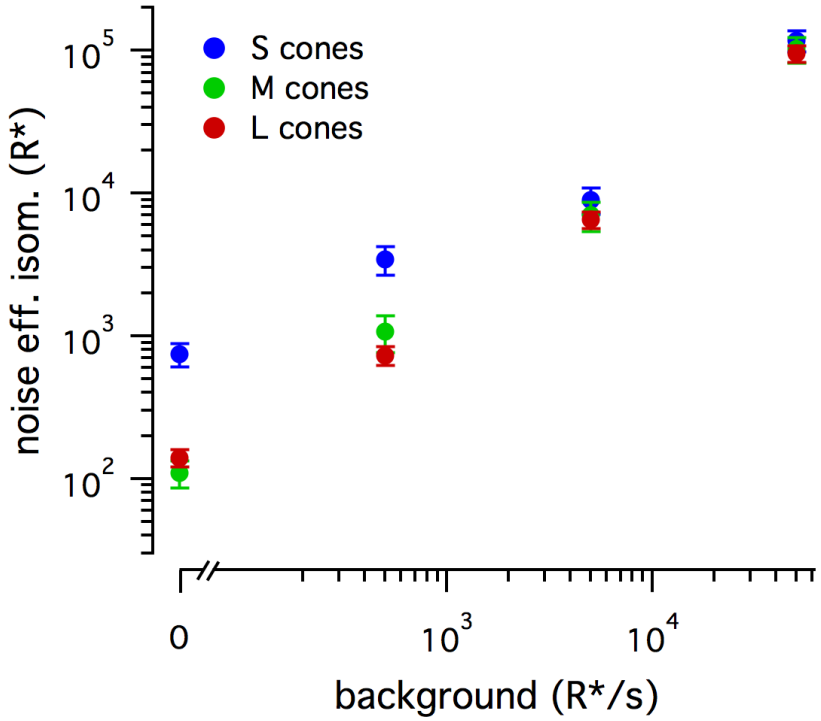

Figure 2.8. Noise effective isomerizations across cone types

Effective noise isomerization levels across backgrounds. Values were computed as number of isomerizations necessary to produce an equivalent power to the noise in the range of 2 to 16 Hz. Points represent mean ± sem. For S cones (n = 9), values were 737 ± 136 R* in darkness, 3422 ± 780 R* at 500 R*/s, 8914 ± 1848 R* at 5,000 R*/s, and 117419 ± 19785 R* at 50,000 R*/s. For M cones (n = 9), values were 110 ± 23 R* in darkness, 3422 ± 780 R* at 500 R*/s, 7050 ± 1624 R* at 5,000 R*/s, and 102721 ± 21195 R* at 50,000 R*/s. For L cones (n = 15), values were 139 ± 19 R* in darkness, 731 ± 110 R* at 500 R*/s, 6522 ± 879 R* at 5,000 R*/s, and 95295 ± 12725 R* at 50,000 R*/s.

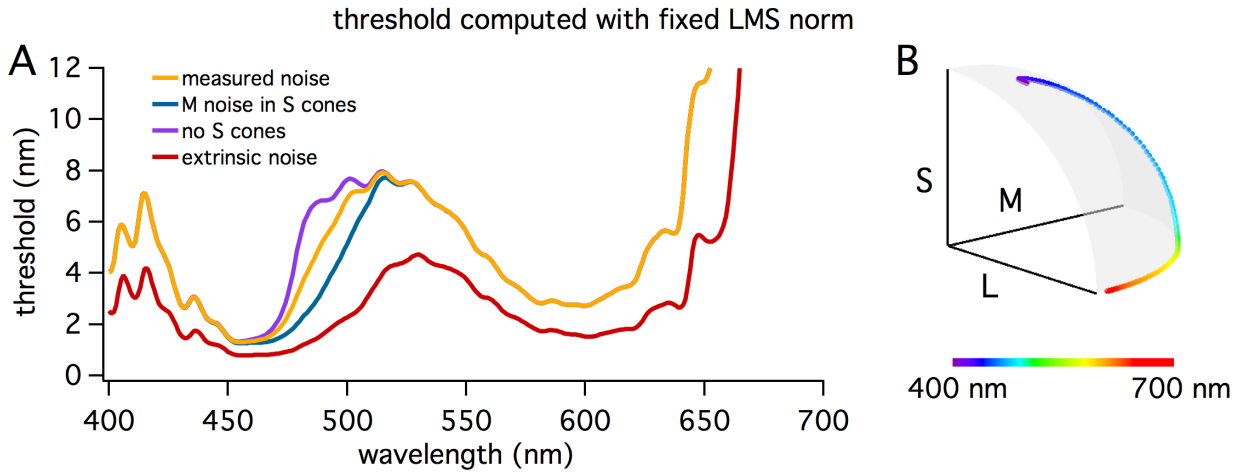

Figure 2.9. Wavelength discrimination, fixed LMS norm

(A) Wavelength discrimination thresholds across the visual spectrum using fixed LMS norm path to determine cone activations at each wavelength (|LMS| = 500 R*, see methods). For a constant LMS norm path, elevated S cone noise hinders discrimination performance from approximately 460 – 510 nm.

(B) LMS space trajectory when LMS norm is held constant for each wavelength. The wavelength range in (A) over which higher S cone noise had a large impact on acuity corresponds to the range over which S cone activation changes considerably on this path through LMS space. Within this range, discrimination will rely on discriminating between LMS space points whose differences are aligned with the noisier S cone dimension, thus limiting acuity.

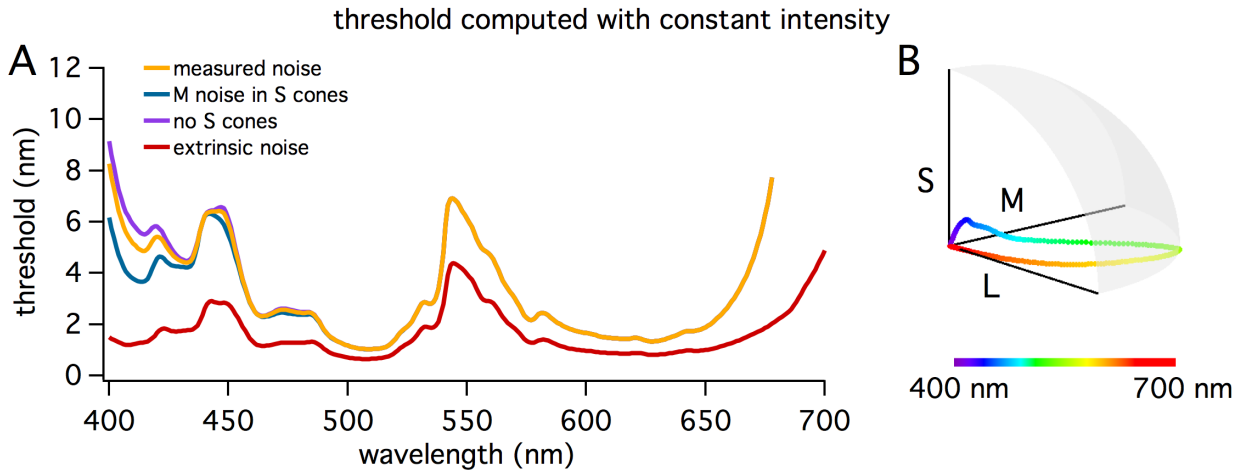

Figure 2.10. Wavelength discrimination, constant intensity

(A) Wavelength discrimination thresholds across the visual spectrum using constant intensity path to determine cone activations at each wavelength (I = 363 photons, see methods). For a fixed intensity path, elevated S cone noise hinders discrimination performance below approximately 440 nm.

(B) LMS space trajectory for fixed intensity stimulus at each wavelength. With a constant intensity path, S cone activations change appreciably only for lower wavelengths. This corresponds to the region in (A) over which elevated S cone noise impacted wavelength discrimination. Within this range, discrimination will rely on discriminating between LMS space points whose differences are aligned with the noisier S cone dimension, thus limiting acuity.

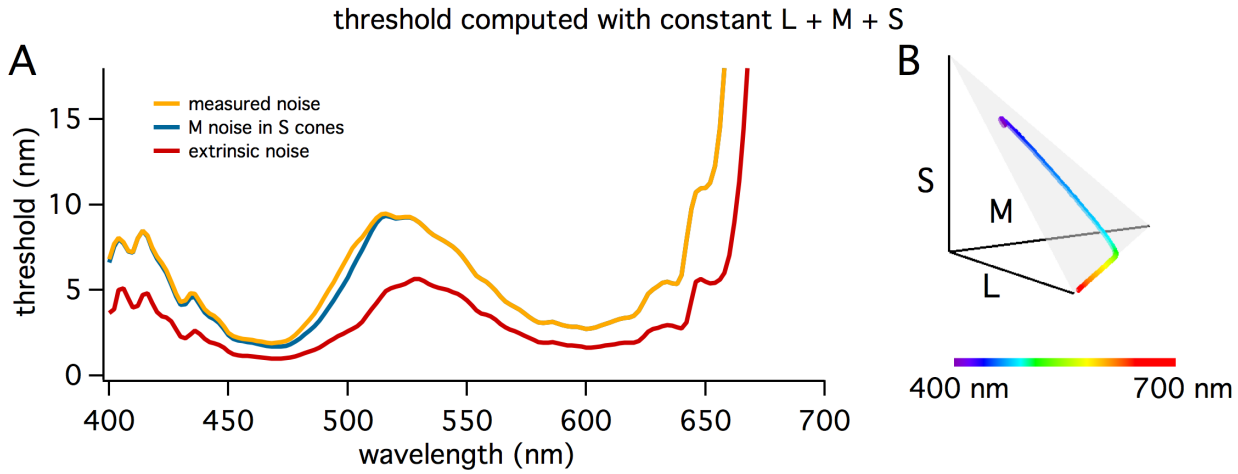

Figure 2.11. Wavelength discrimination, L + M + S plane

(A) Wavelength discrimination thresholds across the visual spectrum using fixed L + M + S sum path to determine cone activations at each wavelength (L + M + S = 500 R*, see methods). For a constant L + M + S sum path, elevated S cone noise hinders discrimination performance from approximately 475 – 510 nm.

(B) LMS space trajectory when L + M + S sum is held constant for each wavelength. The wavelength range in (A) over which higher S cone noise had an impact on acuity corresponds to the range over which S cone activation changes considerably on this path through LMS space. Within this range, discrimination will rely on discriminating between LMS space points whose differences are aligned with the noisier S cone dimension, thus limiting acuity.

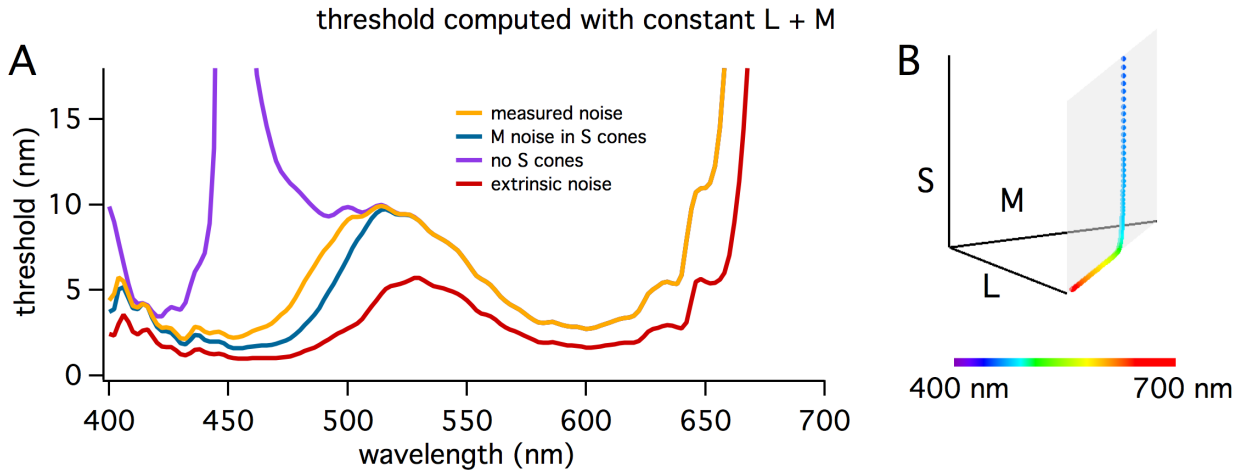

Figure 2.12. Wavelength discrimination, L + M plane

(A) Wavelength discrimination thresholds across the visual spectrum using fixed L + M sum path to determine cone activations at each wavelength (L + M = 500 R*, see methods). For a constant L + M sum path, elevated S cone noise hinders discrimination performance from approximately 440 – 510 nm. Further, the presence of S cones is critical for a region centered at approximately 450 nm.

(B) LMS space trajectory when L + M sum is held constant for each wavelength. The wavelength range in (A) over which higher S cone noise had a large impact on acuity corresponds to the range over which S cone activation changes considerably on this path through LMS space. Within this range, discrimination will rely on discriminating between LMS space points whose differences are aligned with the noisier S cone dimension, thus limiting acuity.

Chapter 3. CONE NOISE ACROSS RETINAL ECCENTRICITY

3.1 ABSTRACT

Primate daylight vision relies heavily on signals generated in cone photoreceptors within the fovea, a specialized region in the central-most retina with high spatial and chromatic acuity. Despite known differences in perceptual sensitivity across the visual field, cones are generally assumed homogeneous throughout the retina. To test this assumption, we measured response properties in foveal, central, and peripheral cones and found that their kinetics change in a graded manner across eccentricity and that these differences persist across background light levels. We also show that peripheral cones transmit more information than foveal cones, especially for higher temporal frequency stimuli. Further, we find that differences across the retina in the signal and noise properties of cones explain previously seen graded changes across the visual field in perceptual sensitivity to temporally modulated stimuli.

3.2 INTRODUCTION

Decades of psychophysical work demonstrates that the performance of our visual system varies across the visual field (Hecht & Verrijp, 1933; Tyler, 1987). How much of this is attributable to differences across eccentricity in the properties of the first neurons of the visual system, the cone photoreceptors? There is an emerging appreciation for diversity in the properties of cones throughout the primate retina, with recent work finding significant differences in the responses of cones from different retinal locations (Sinha *et al.*, 2017). Foveal long (L) and medium (M) wavelength sensitive cones generate responses that are slower than their peripheral counterparts by approximately a factor of 2. These differences have direct perceptual implications because although the fovea covers <1% of the retinal surface area, it provides ~50% of both the output of

the retina and the input to visual cortex (Wässle *et al.*, 1989). Both at the retinal output and perceptually, foveal vision is known to have lower sensitivity to rapidly varying inputs compared to peripheral vision, agreeing well with the cone kinetic differences (Hecht & Verrijp, 1933; Solomon *et al.*, 2002; Sinha *et al.*, 2017).

The initial work comparing foveal and peripheral cones focused on a narrow range of stimulus conditions, namely flash responses at a single background light level (Sinha *et al.*, 2017). Three particularly salient questions are motivated by these findings. First, natural cone inputs are diverse and peripheral cone responses are known to change across different inputs (Schnapf *et al.*, 1990; Angueyra & Rieke, 2013; Cao *et al.*, 2014). How do signals generated in foveal and peripheral cones compare across this range of stimuli? Second, eccentricity-dependent perceptual differences in temporal sensitivity change in a graded manner across the visual field (Hecht & Verrijp, 1933; Tyler, 1987). Do foveal and peripheral cones form two classes of cone photoreceptors with a discrete boundary, or do cone properties vary in a similar, graded manner across eccentricity? Finally, as in any primary sensory neuron, cone signals exist in the presence of noise (Rieke & Baylor, 2000; Angueyra & Rieke, 2013). To directly relate differences in cone signals to visual system performance, it is essential to interpret them in the context of their noise. Do the noise properties of primate cones vary across eccentricity?

We recorded from primate cones in foveal, central, and peripheral retina across a range of background light levels and compared their signal and noise properties. We found that cone kinetic properties change in a graded manner across eccentricity, and that these differences persist across a range of background light levels. By reconstructing cone stimuli from their responses we show that peripheral cones transmit more information than foveal cones overall and especially at higher frequencies. We also found that differences in cone signal and noise properties across the retina

predict eccentricity-dependent differences in the perception of flickering stimuli that agree quite well with those observed in past psychophysical measurements.

3.3 RESULTS

The results below are divided into 4 sections: (1) characterization of cone kinetics across background light levels and eccentricity; (2) comparison of cone noise properties across eccentricity; (3) stimulus reconstructions using foveal and peripheral cone responses; and (4) evaluation of the impact of differences in signal and noise in cones across eccentricity on flicker detection thresholds.

3.3.1 *Cone kinetics show graded changes across eccentricity*

Foveal cone flash responses are considerably slower than those of peripheral cones (Sinha *et al.*, 2017). Is there a discrete boundary across eccentricity at which cones transition from having slower foveal kinetics to faster peripheral kinetics, or does this transition occur in a graded manner? To answer this question, we recorded L and M cone voltage responses to brief flashes in foveal (<500 μm from foveal pit), central (1500 - 2500 μm from foveal pit), and peripheral (>5000 μm from foveal pit) retina (Figure 3.1A, B). Central cones had kinetics that were intermediate to those of foveal and peripheral cones (Figure 3.1C).

Responses of peripheral cones accelerate with increasing background light level (Dunn *et al.*, 2007; Angueyra & Rieke, 2013). This suggests that eccentricity-dependent kinetic differences may depend on background light level. To test for such a dependence, we recorded flash responses at all three eccentricities across a range of background light levels (Figure 3.1D). We quantified kinetics at each background from the times to peak of the cone responses. Across eccentricities, the times to peak fell as the background light level increased, demonstrating that central and foveal

cone light responses also accelerate. Furthermore, under the conditions we tested the kinetic changes with background were quite similar across eccentricity, thus leaving the differences in times to peak across eccentricity relatively constant. This suggests eccentricity and background light level have independent effects on cone kinetics.

To confirm the graded kinetic difference we observed in flash responses across eccentricity, we measured cone responses to sinusoidal stimuli across a range of frequencies. Cones with slower kinetics would be expected to generate weaker responses to stimuli with rapid temporal modulation. In each cone, we constructed a frequency tuning curve showing the cone's response amplitude per unit of stimulus contrast across frequencies (Figures 3.1E, F). The average frequency tuning curves show that foveal response gain is the weakest at higher frequencies, peripheral gain is the strongest, and central cones fall between them. To quantify flicker sensitivity in individual cones, we found the frequency at which their response gain had fallen by an order of magnitude from its maximum (Figures 3.1E, F, insets). This frequency increased progressively with increasing eccentricity, providing additional support for the finding that cone kinetics change in a graded manner across eccentricity

3.3.2 *Noise in cones across eccentricity*

Cones' ability to transmit information to downstream circuitry depends on both their signals and noise. There is a history of measurements of signal and noise within photoreceptors providing insight into perception (Donner, 1992; Field *et al.*, 2005; Angueyra & Rieke, 2013). Despite signals from foveal and central retina providing greater than half the input to primate visual cortex, signal and noise comparisons have not been made at these eccentricities. The kinetic differences we find across eccentricity motivate making noise measurements in foveal and central cones directly.

We recorded cellular noise in cones across eccentricity and background light levels as done in Angueyra & Rieke, 2013 (Figure 3.3). As previously seen in peripheral primate and salamander retina, noise in foveal and central cones changed across background light levels (Figure 3.3; Angueyra and Rieke, 2013; Rieke and Baylor, 2000). For each eccentricity and background, we compared the measured noise to the dim flash response (Figure 3.2A-C). Across eccentricities, the frequency range of cellular noise extended beyond that of the flash response. We quantified noise power by integrating over two frequency ranges, one overlapping with the flash response spectrum and the other at higher frequencies. We refer to these ranges as the flash response and high frequency ranges (Figure 3.2A-C).

Previous work in peripheral L and M cones measured cellular noise in darkness and across a range of light levels (Angueyra & Rieke, 2013). On dim backgrounds, noise power at frequencies overlapping with the flash response increased to approximately twice that in darkness before falling well below the noise in darkness as backgrounds increased further. Foveal and central cone noise also behave similarly across backgrounds (Figure 3.2D). This increased noise at dimmer backgrounds has been attributed to increased Poisson noise in photon absorption prior to significant adaptation in the light response. In agreement with this mechanism, peripheral cone noise beyond the flash response range does not show increased noise at low light levels (Angueyra & Rieke, 2013). This is also the case in foveal and central cones (Figure 3.2E).

These comparisons of noise power across backgrounds describe how cone noise changes across different stimulus conditions. It is also important to directly compare the signal and noise power at each background. To relate our signal and noise measurements to perception, we predicted cone detection thresholds across backgrounds at each eccentricity. These thresholds were defined as the flash strengths necessary to produce a response whose power matched the noise

power between 1 Hz and 60 Hz in a 200 ms integration window. Across backgrounds, detection thresholds were quite similar at all eccentricities (Figure 3.2F).

3.3.3 *Foveal cones carry less stimulus information, especially at higher frequencies*

Flash detection thresholds likely rely heavily on lower frequency components of the flash response, which is the region of greatest similarity across eccentricity. However, natural visual inputs are temporally modulated on a range of timescales, making it important to consider how effectively cones transmit information across a breadth of conditions. Differences in response kinetics and frequency tuning of cones across eccentricity suggest that differences in their ability to transmit information will be most pronounced for stimuli undergoing more rapid temporal modulation. How does information transfer as a function of frequency vary in cones across eccentricity?

Reconstructing stimuli from a cell's responses allows its information transmission to be quantified. Any information about the true stimulus present in the reconstructed stimulus must have been present in the neuron's responses. Errors in stimulus reconstructions can be used to calculate a lower bound on the signal to noise ratio of a neuron's response as a function of frequency (Bialek *et al.*, 1991, 1993). We applied this analysis to responses to Gaussian noise stimuli in both peripheral and foveal cones.

We reconstructed cone stimuli using a linear-nonlinear model in which the inputs were cone responses and the outputs were the stimuli generating those responses (Figure 3.4A). As expected based on differences in the power spectra of foveal and peripheral cone responses (Figure 3.4B), peripheral reconstructions appeared to capture more high frequency content than foveal reconstructions (Figure 3.4C). When information transfer was quantified as a function of frequency, there were two main differences across eccentricity: (1) across all frequencies,

peripheral cones transmitted more information (Figure 3.4D); and (2) information transfer in peripheral cones extended to much higher frequencies than in foveal cones (Figure 3.4D, inset). Overall information transmission was approximately twice as high in peripheral cones (Figure 3.4E).

3.3.4 *Cone properties can explain flicker fusion differences across eccentricity*

Foveal cones transmit less information than peripheral cones, especially at higher frequencies (Figure 3.4, Figure 3.5A). This agrees well with past psychophysical work measuring critical flicker fusion frequencies across the visual field (Hecht & Verrijp, 1933; Tyler, 1987; Snowden & Hess, 1992). This is the frequency at which a flickering light appears solid, and reflects the point at which the rate of temporal modulation of a stimulus exceeds the ability of the visual system to respond. Flicker fusion frequencies are lowest in the central-most (or foveal) visual field, and progressively increase as eccentricity increases (Hecht & Verrijp, 1933; Tyler, 1987; Snowden & Hess, 1992). Can differences in cone properties across eccentricity explain these perceptual differences?

To assess the impact of cone differences on flicker fusion, we used our measurements of signal and noise to predict flicker fusion frequencies from ideal observer models constructed for each eccentricity (Geisler, 1989). We defined the flicker fusion frequency as the highest frequency at which a 100% contrast sinusoidal stimulus was detectable. To facilitate comparison with psychophysical flicker fusion measurements across eccentricity (Tyler, 1987), our ideal observer had access to signals from 5,000 cones. Signals were considered detectable if the overall signal to noise ratio (SNR) was 1.0. It is impossible to know a psychophysics observer's exact threshold SNR. A target SNR of 1.0 was chosen to align the magnitude of our predictions with psychophysical measurements. Had we chosen a higher target SNR, our predicted flicker fusion

frequencies would all decrease. Had the SNR been lower, they would all increase. This dependence on the selected SNR suggests that our predictions should only be used to evaluate the eccentricity dependence of flicker fusion frequencies, not their absolute magnitudes.

We assumed the only prior knowledge available to the observer was that the stimulus frequency would be between 1 and 100 Hz with a random phase. Under these assumptions, the signal power in a single cone is the power spectrum of the cell's response integrated between 1 and 100 Hz. Responses were calculated as the stimuli convolved with an estimate of the single photon response from our measurements. The noise power in a single cone is the noise power spectrum integrated between 1 and 100 Hz. Under this model, the SNR across 5,000 cones is 5,000 times the SNR in a single cone.

Our models' predictions are in close alignment with past psychophysical work. With increasing eccentricity, flicker fusion frequencies increased by an amount comparable to that seen in psychophysical measurements (Tyler, 1987; Figure 3.5B). Also in agreement with past measurements, flicker fusion frequencies increased with increasing background light levels (Brindley *et al.*, 1966; Marks & Bornstein, 1973).

3.4 DISCUSSION

3.4.1 *Implications of cone differences for study of the visual system*

Studies of the retina strive to explain the computations performed by the underlying circuitry and understand the neural mechanisms by which they are implemented. This generally involves recording at different points within the circuitry to characterize the relationship between stimuli and cells' responses. The computations giving rise to these responses reflect the culmination of processing occurring at all upstream steps that carry the signal. Cones have classically been assumed to be functionally homogeneous, leading differences in downstream responses to be

attributed solely to circuit-level mechanisms. There is accumulating evidence for functional diversity of cones in primate and it will be important to incorporate these differences into the interpretation of future work in the retina. Developing a more thorough understanding of differences between foveal and peripheral cones, as well as intermediate eccentricities, is therefore essential for both studies of retinal circuitry as well as the interpretation of perceptual experiments in the context of visual system circuitry.

3.4.2 *Cone kinetics change in a graded manner across eccentricity*

Past work observed kinetic differences in foveal and peripheral cones (Sinha *et al.*, 2017). These differences could be explained by the presence of two distinct populations of cones in foveal and peripheral retina, or by cone properties progressively changing across eccentricity. Resolving this distinction was important because it allows cone responses to be more accurately predicted across all eccentricities. We find that cone response kinetics become progressively faster with increasing eccentricity, which motivates caution when interpreting downstream retinal responses across eccentricities. Care must be taken to differentiate between differences in response properties originating in the cones and those that are introduced by differential downstream processing. It is important to incorporate graded changes in cone response properties into retinal models and use them to inform the interpretations of measurements in downstream circuitry or perception, both in future work and when revisiting that of the past.

The fovea is a specialization of the primate visual system allowing high spatial and chromatic acuity vision. Both the mechanistic and evolutionary origins of slower foveal cones remain unknown. One possibility is that, given the statistics of natural inputs and eye movement dynamics, they improve the encoding of visual inputs. An alternative possibility is that they are a tradeoff necessitated by anatomical differences, such as significantly longer foveal axons, that

allow high cone density in the central-most retina (Hsu *et al.*, 1998). Future work should aim to address these questions.

3.4.3 *Cone signals and noise explain perception across eccentricity*

Initial measurements of cone noise predicted cone detection thresholds far greater than those measured psychophysically (Donner, 1992; Koenig & Hofer, 2011). More recent work found improved signal to noise ratios in cones, and predicted thresholds quite similar to those from psychophysics (Angueyra & Rieke, 2013). One remaining confound in connecting physiology to perception is that these cone noise measurements were made in peripheral primate retina, while the psychophysics targeted the fovea. Our recordings directly confirm that cone dim flash detection thresholds are similar in foveal and peripheral retina. Further, our cone detection threshold predictions at all three eccentricities are lower than previous peripheral predictions, making them lower than what has been measured psychophysically. Differences between thresholds measured psychophysically and those predicted from cone recordings place constraints on the operation of downstream circuitry. If they are the same, it suggests the downstream circuitry operates effectively noiselessly. We find that cone detection thresholds across eccentricity are lower than what has been seen in both neurons from visual cortex and psychophysics, in agreement with past work showing that downstream circuitry further limits perception (Hass *et al.*, 2015).

Vision in the central-most part of the visual field has been known to be sluggish for decades (Hecht & Verrijp, 1933). Previous electroretinogram measurements suggested this could be due to kinetic differences in the cones themselves, but this was only recently validated with direct single-cell foveal cone recordings (Seiple & Holopigian, 1996; Sinha *et al.*, 2017). These initial recordings were at a single background light level and did not include the noise measurements necessary to fully relate cone properties to perception. Our measurements of signal and noise

across eccentricity and backgrounds allowed us to construct an ideal observer model and make predictions of critical flicker fusion limits established in the cones themselves. Although uncertainty about the SNRs required for flicker detection by psychophysics observers confounds interpretation of the absolute magnitudes of the predicted frequencies, comparisons across eccentricity are still valid and quite informative. We find that differences in cone properties across eccentricity well explain the structure of differences in flicker fusion frequency across the visual field. This could arise in two ways: (1) differences in cones themselves account for virtually all of the differences in perception, and downstream responses are limited by cone properties; or (2) cone performance exceeds that of perception, but downstream circuitry across eccentricity reads these signals out with near identical fidelity. It will be interesting to see if this and other perceptual differences across the visual field can be explained simply by differences in cones themselves.

3.5 METHODS

3.5.1 *Tissue, cells, solutions*

Electrophysiological recordings were performed on primate retina from the Tissue Distribution Program of the University of Washington's Regional Primate Research Center. Recordings were made from retinas from *Macaca fascicularis, Macaca nemestrina,* and *Macaca mulatta* of both sexes, aged 2 through 20 years. All primate tissue use was done in accordance with the University of Washington Institutional Animal Care and Use Committee. Tissue was obtained and prepared as described previously (Angueyra & Rieke, 2013; Sinha *et al.*, 2017). In short, dark adapted (> 1 hour) retina stored in warm (~32° C), oxygenated Ames medium was placed photoreceptor side up on a poly-lysine-coated coverslip (BD Biosciences) that served as the floor of our recording chamber. Throughout recordings, the retina was continuously perfused with warm, oxygenated Ames solution.

3.5.2 *Patch-clamp recordings*

Cone patch clamp recordings were performed as described previously (Angueyra & Rieke, 2013; Sinha *et al.*, 2017). In short, we measured cone light responses using whole-cell current clamp (holding current = 0 pA) or voltage clamp (holding current = -60 mV) recordings. Data were low pass-filtered at 3 kHz, digitized at 10 kHz, and acquired using a Multiclamp 700B amplifier. All recordings were controlled using the MATLAB-based Symphony Data Acquisition Software, a piece of open-source electrophysiology software (https://github.com/symphony-das).

3.5.3 *Light stimulation*

Stimuli were presented using computer-driven LEDs with peak wavelengths of 406, 515, and 640 nm to allow effective stimulation of all 3 cone types. Light stimuli covered a ~500 μm disk centered on the cell being recording from. All stimulus protocols were generated using custom-written MATLAB-based extensions of Symphony Data Acquisition Software, and delivered at 10 kHz. To determine cone isomerization rates, we used measured LED power output, measured LED spectra, primate photoreceptor spectra from Baylor et al., 1987, and an effective collecting area of 0.37. μm^2 (Schnapf *et al.*, 1990).

3.5.4 *Analysis*

All analysis was performed using custom-written MATLAB analysis routines.

Times to Peak: Times to peak were calculated from a cell's average response to repeated dim flashes. To account for any noise in the responses around the peak, we used a fitting-based approach to calculate the times to peak. Each average response was fit with the following equation that has been shown to successfully capture the dynamics of the cone light response (Angueyra & Rieke, 2013):

$$f(t) = \alpha \times \left[\frac{(\frac{t}{t_{rise}})^4}{1+(\frac{t}{t_{rise}})^4}\right] \times \left[e^{-\left(\frac{t}{t_{decay}}\right)}\right] \times \left[cos(\frac{2\pi t}{t_{osc}} + \phi)\right] \qquad (3.1)$$

Times to peak were taken to be the time at which the fit equation reached its maximal value.

Spectral Analysis: Power spectra for noise and flash responses were computed using MATLAB's built-in fast Fourier transform, followed by conversion to a two-sided power spectral density with units of pA^2/Hz. Recorded dim flash responses contain contributions from the flash response, cellular noise, and instrumental noise. To isolate the flash response, recordings were fit using Equation 3.1. The flash response power spectrum was then taken to be the power spectrum of this fit. To calculate signal or noise power in a given frequency range, power spectral densities were integrated across the range.

Noise Isolation: Cellular noise was isolated as described previously (Angueyra & Rieke, 2013). Noise in cone current measurements from voltage clamp recordings contains contributions from noise arising within phototransduction in the cones (cellular noise), and from the recording itself (instrumental noise). When a near-saturating light stimulus is delivered to the cones, it will shut down phototransduction and eliminate virtually all cellular noise, leaving only instrumental noise. Assuming cellular and intrinsic noise are independent and additive, cellular noise at a given background light level can be isolated by subtracting the power spectrum of noise during saturation from the power spectrum of the measured noise at that background.

Frequency Tuning Curves: Frequency tuning curves quantified a cone's responses to sinusoidal stimuli across frequencies. To construct a curve, a cone's mean responses to stimuli of each frequency were fit with the following equation:

$$y = a * sin(2\pi * fx + b) + c \qquad (3.2)$$

For the fit, f was matched to the frequency of the stimulus, while a, b, and c were free to vary. Once the fits were obtained, the value of a for each frequency was divided by the contrast of the

stimulus at that frequency to arrive at a final value for the cell's sensitivity at that frequency. Normalizing by the contrast was necessary because higher contrast stimuli were required to elicit responses at frequencies to which the cell was less sensitive.

Tuning curves were compared across the population by calculating the frequency at which a cone's gain had dropped by a factor of 10 from its maximal value. This was calculated by interpolating a fit of the frequency tuning curve to the power spectrum of Equation 3.1. Under an assumption of linearity, the frequency tuning curve is proportional to the flash response power spectrum, which makes this a reasonable function to use for interpolation. Best fits were those that minimized the following loss function:

$$L(\theta) = \sum_i \left| log(\frac{F(\omega_i,\theta)}{D(\omega_i)}) \right| \qquad (3.3)$$

Here, $F(\omega_i, \theta)$ is the prediction from a fit with parameters θ at the frequency ω_i, and $D(\omega_i)$ is the data.

Stimulus Reconstruction: Stimulus reconstruction was performed as described previously (Rieke *et al.*, 1997). In short, if a cell's response is used to reconstruct a stimulus, any information about the true stimulus present in the reconstructed stimulus must have also been present in the cell's response. This approach can be used to place a lower bound on the information about the true stimulus present in the response.

To perform this analysis, responses to segments of white noise stimuli were recorded. The stimulus for each segment was predicted by fitting a linear-nonlinear (LN) model to the remaining segments (for details of construction, see Kim and Rieke, 2001), and using it to predict the stimulus for the held out segment. Errors in each prediction were calculated and moved to the frequency domain. As done previously (see Rieke et al., 1993, 1997), these errors were divided into random

and systematic components. Using the signal power spectrum and calculated noise powers as a function of frequency, information transfer (in units of bits) can be calculated as (Shannon, 1949):

$$I = \int_{-\infty}^{\infty} \frac{d\omega}{2\pi} log_2 \left[1 + \frac{S(\omega)}{N(\omega)}\right] \qquad (3.4)$$

This information represents a lower bound on the information present about the stimulus in a cell's responses.

Flicker Detection Threshold Calculation: Flicker fusion occurs when an observer perceives a flickering stimulus as constant (Hecht & Verrijp, 1933; Tyler, 1987). We predicted flicker fusion thresholds for an ideal observer with access to signals in 5,000 cones. 5,000 was chosen to make our predicted frequencies span a range comparable to that in Tyler, 1987 with a reasonable SNR threshold. In our model, a stimulus was considered detectable if its response had a SNR greater than 1 in an integration time of 1 second. It is impossible to know the exact decision criteria used by observers in a psychophysical task, making the SNR for detectability an unconstrained parameter. We used 1 because it yielded predictions quite similar to the values measured by Tyler, 1987 and facilitated comparison to this work. The absolute magnitudes of our predicted frequencies depend strongly on SNR used. Thus, the uncertainty in observer SNR thresholds means our predictions should only be used for comparisons of the structure of flicker fusion across eccentricity and background light levels, because the same SNR was used at each eccentricity and background.

Flicker fusion was defined as a 100% contrast sinusoidal stimulus being undetectable (SNR < 1). In our calculations of detectability, we assumed the observer did not know the frequency or the phase of the stimulus. The only prior information they had access to was that the stimulus would fall between 1 and 100 Hz. The observer's task was to determine if there was or was not a stimulus on a given trial. Under these assumptions, the noise power on a given trial will be the

integral of the noise power spectrum between 1 and 100 Hz. The signal will be the power spectrum of a cell's response integrated over the same range. A cell's response was taken to be the stimulus convolved with the estimated single photon response (from measured dim flash responses). The SNR in a single cell was the integral of the signal spectrum divided by the integral of the noise spectrum. The SNR will scale linearly with the number of cones, meaning the SNR in a patch of 5,000 cones is 5,000 times greater than that of a single cone. Using this approach to calculate the SNR in the patch of cones, we determined the frequency at which the SNR fell below 1, which was taken to be the flicker fusion frequency.

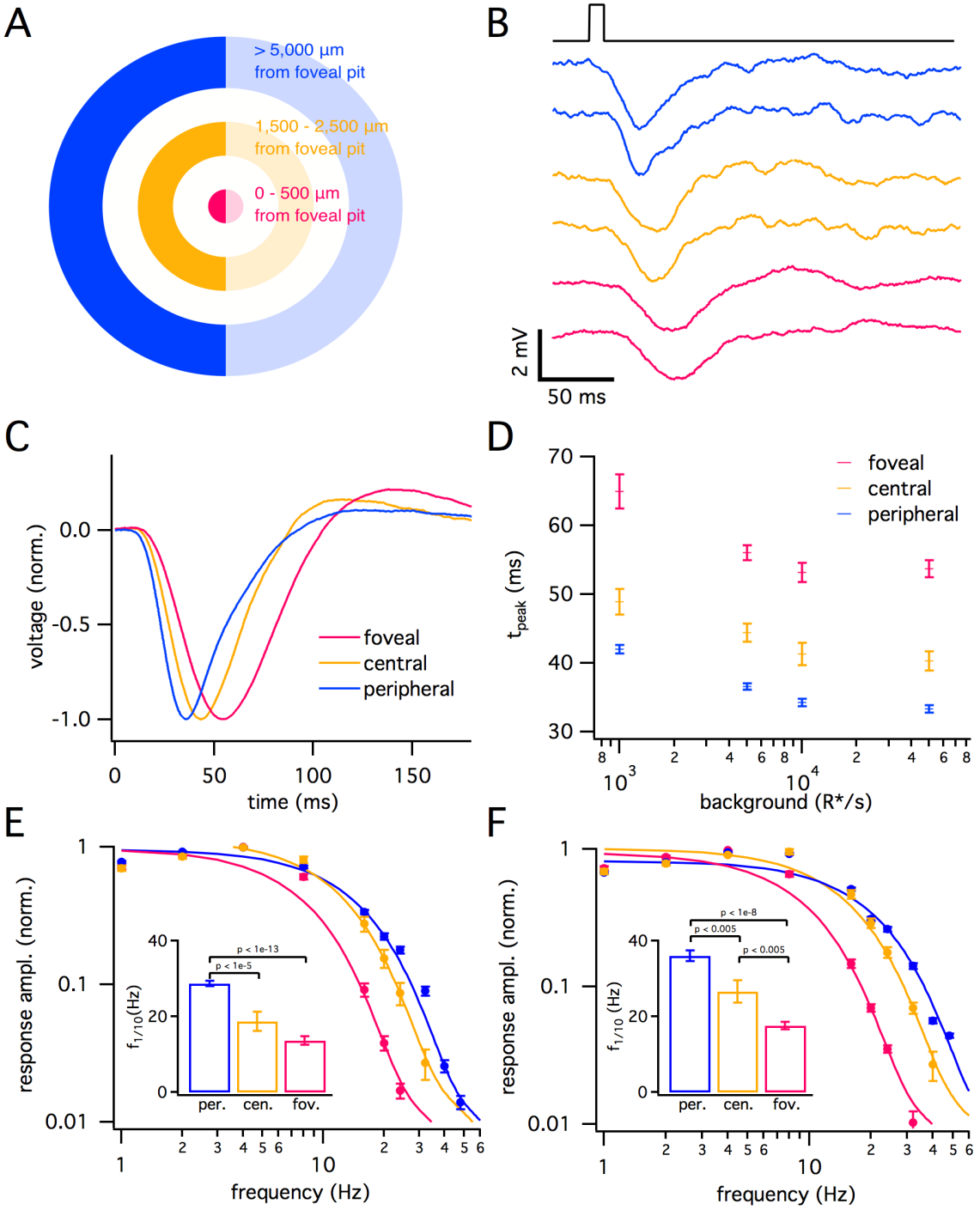

Figure 3.1. Cone kinetics change in a graded manner across eccentricity

(A) Schematic showing eccentricity definitions and colors used throughout figures. Measured from the center of the foveal pit, 0 - 500 µm was defined as foveal (magenta), 1,500 - 2,500 µm was defined as central (gold), and >5,000 µm was defined as peripheral (blue).

(B) Example raw current clamp responses of exemplar peripheral, central, and foveal cones to a 10 ms flash giving on average 150 absorbed photons (R*). Flashes were delivered on a background of 5,000 R*/s.

(C) Average normalized flash responses across cells in foveal, central, and peripheral retina to stimulus described in (B).

(D) Mean ± sem times to peak of flash responses in foveal, central, and peripheral retina across background light levels. At 1,000 R*/s, mean ± sem times to peak were 65.0 ± 2.4 ms, 48.9 ± 1.9 ms, and 42.0 ± 0.7 ms in foveal, central, and peripheral retina, respectively. At 5,000 R*/s, they were 56.0 ± 1.0 ms, 44.4 ± 1.3 ms, and 36.6 ± 0.4 ms. At 10,000 R*/s, they were 53.2 ± 1.4 ms, 41.3 ± 1.6 ms, and 34.2 ± 0.5 ms. At 50,000 R*/s, they were 53.7 ± 1.2 ms, 40.3 ± 1.4 ms, and 33.3 ± 0.5 ms.

(E) Frequency tuning curves from cones at each eccentricity on a background of 5,000 R*/s. Points with error bars show mean ± sem normalized response amplitudes across frequencies. Curves show best fit of power spectrum of Equation 3.1 to population data. Inset shows mean ± sem frequencies across the population at which response amplitudes fell to 10% of their maximum value. These are 13.6 ± 1.1 Hz in foveal cones, 18.8 ± 2.5 Hz in central cones, and 28.7 ± 0.7 Hz in peripheral cones.

(F) As in (E), but on a background of 50,000 R*/s. Frequencies for 10% maximal responses are 17.6 ± 0.9 Hz in foveal cones, 26.7 ± 2.9 Hz in central cones, and 36.0 ± 1.4 Hz in peripheral cones.

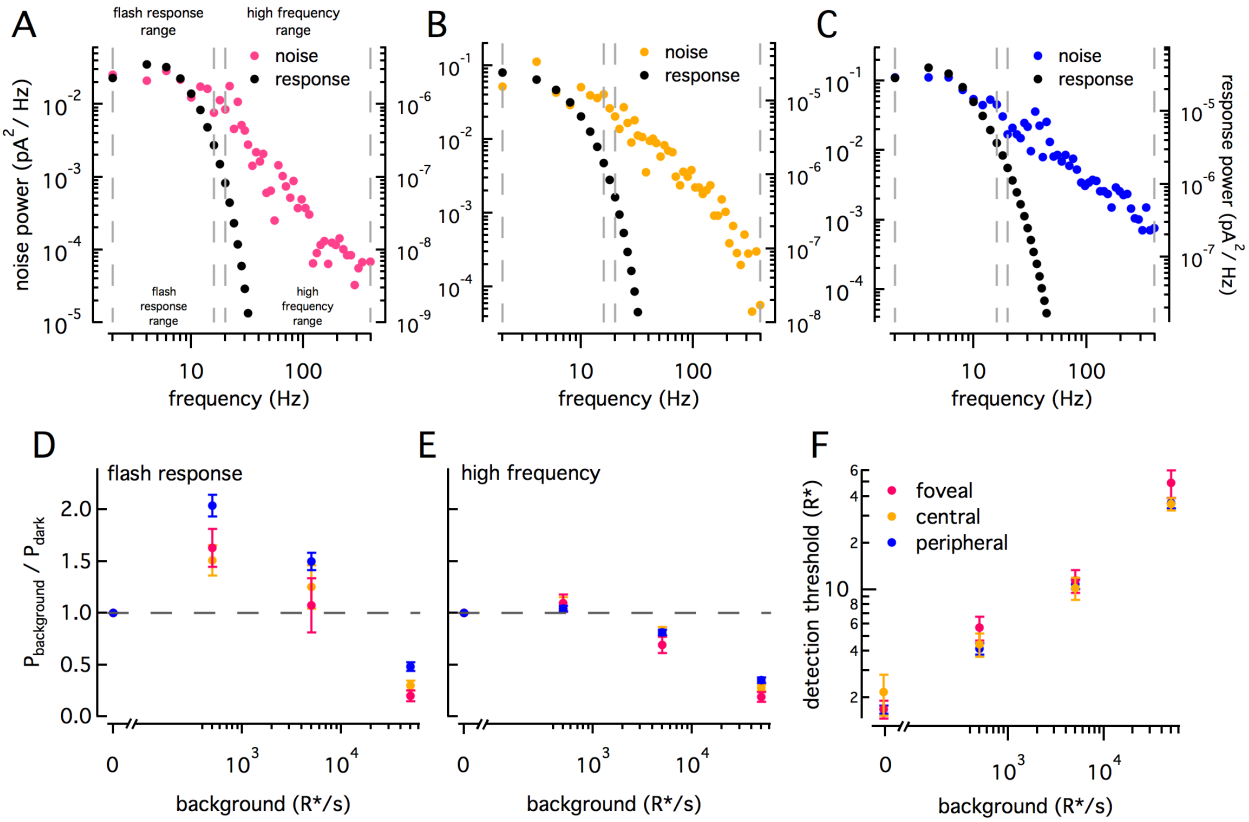

Figure 3.2. Cone noise across eccentricity

(A-C) Signal and noise power spectra in example foveal (A), central (B), and peripheral (C) cones. Spectra with colored markers (left axes) are those of isolated cellular noise. Spectra with black markers (right axes) are those of fit single photon response predictions at each eccentricity. Dashed grey lines show definitions of flash response and high frequency ranges.

(D) Noise power in flash response range across backgrounds. Values are mean ± sem powers at each background normalized by power in darkness. Dashed line shows noise power in darkness.

(E) As in (D) for high frequency range.

(F) Detection thresholds across eccentricities at a range of background light levels. Values are mean ± sem. In darkness, mean ± sem thresholds were 2.7 ± 0.4 R*, 3.5 ± 1.0 R*, and 2.7 ± 0.2 R* in foveal, central, and peripheral cones, respectively. At 500 R*/s, they were 9.1 ± 1.6 R*, 7.1

± 1.2 R*, and 6.6 ± 0.6 R*. At 5,000 R*/s, they were 18.3 ± 3.1 R*, 16.3 ± 2.7 R*, and 17.4 ± 1.3 R*. At 50,000 R*/s, they were 78.8 ± 15.8 R*, 57.7 ± 5.3 R*, and 58.0 ± 4.5 R*.

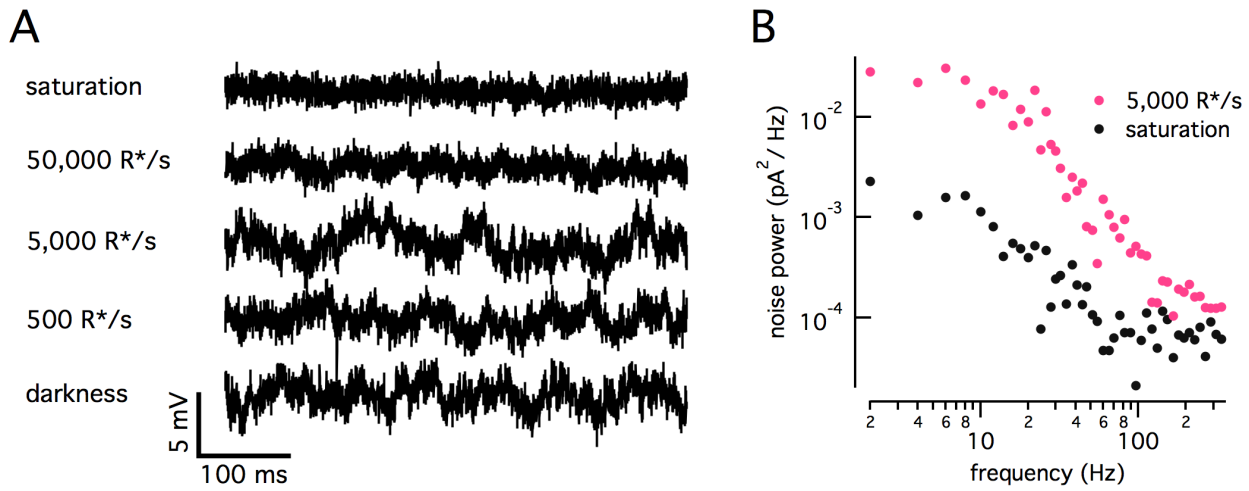

Figure 3.3. Isolating cone cellular noise

(A) Example raw noise measurements from a foveal cone across background light levels and in the presence of saturating light.

(B) Combined extrinsic and cellular noise from example foveal cone at background of 5,000 R*/s (magenta), and isolated extrinsic noise in presence of saturating light (black).

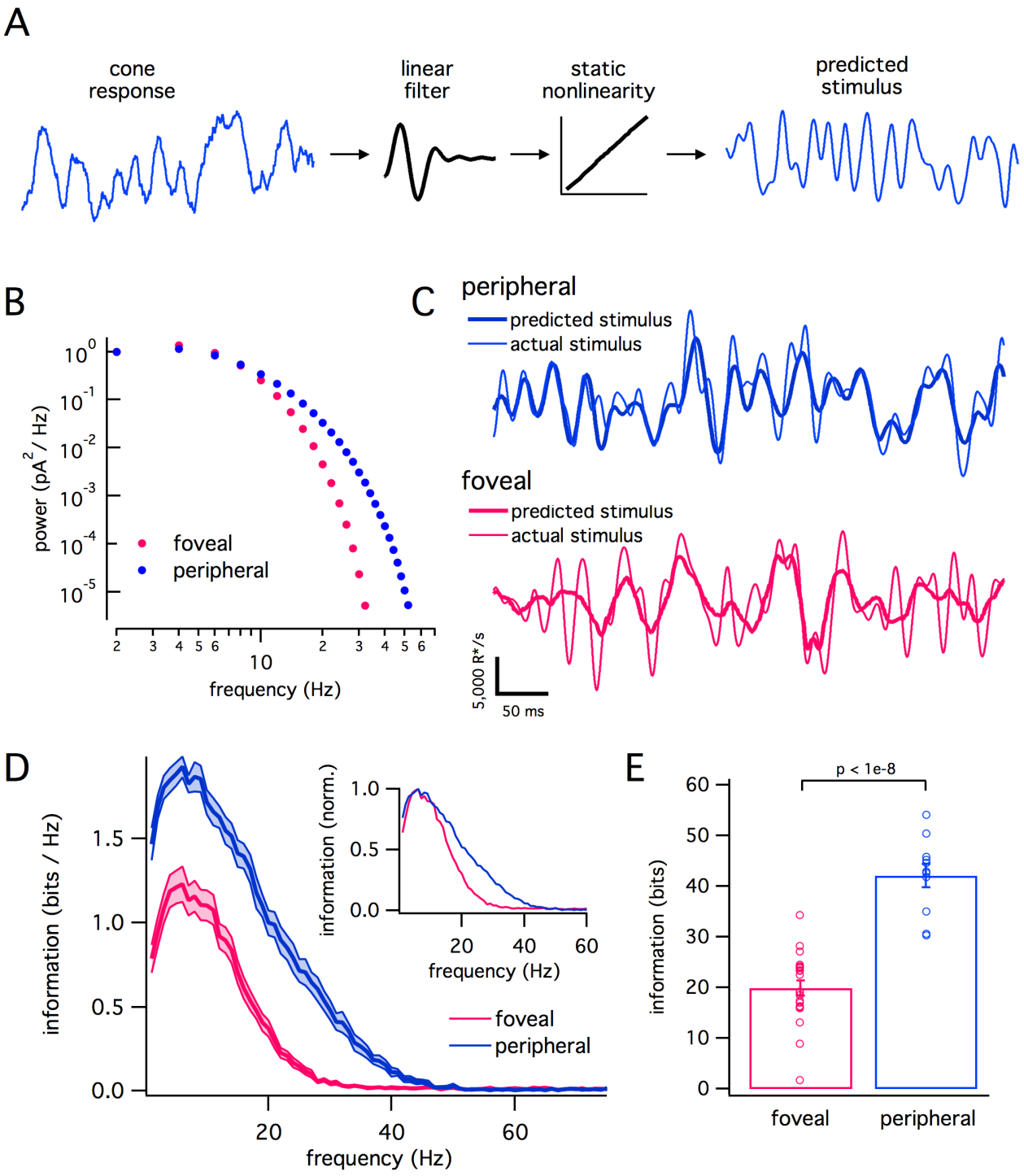

Figure 3.4. Peripheral cones transmit more information, especially at high frequencies

(A) Schematic of stimulus reconstruction process (see Methods). Stimuli were predicted from cone responses using a linear filter and static nonlinearity fit to other responses from the same cell.

(B) Normalized average flash response power spectra at 5,000 R*/s from foveal and peripheral cones.

(C) Example stimulus predictions and actual stimuli from example foveal and peripheral cones demonstrating that stimuli reconstructed from peripheral cones capture more of the rapid temporal modulation in the true stimulus.

(D) Transmitted information across frequencies in foveal and peripheral cones. Shaded regions are ± sem. Inset shows the same curves normalized to have the same peak amplitude and shows the more rapid fall in information transfer in foveal cones as frequency increases.

(E) Total information about stimulus below 60 Hz in responses of foveal and peripheral cones. Error bars are ± sem. Mean ± sem information was 19.9 ± 1.5 bits in foveal cones and 42.1 ± 2.3 bits in peripheral cones.

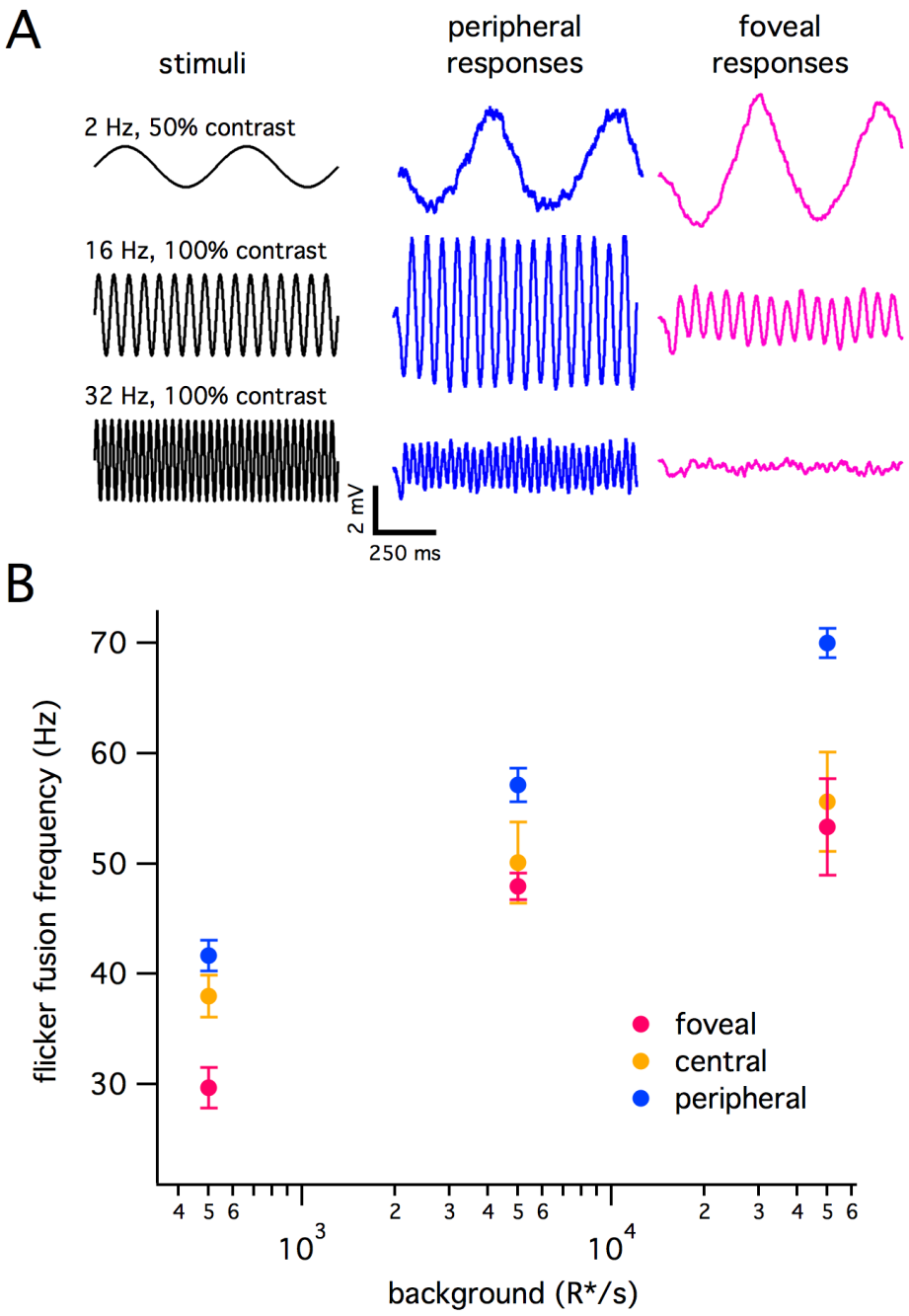

Figure 3.5. Cone properties explain perceptual differences across eccentricity

(A) Responses from an example peripheral (blue) and foveal (magenta) cone to sinusoidal stimuli (black) at 2, 16, and 32 Hz delivered on a background 50,000 R*/s. Responses demonstrate relative inability of foveal cones to respond to rapid temporal modulation.

(B) Critical flicker fusion frequency predictions across backgrounds and eccentricities from an ideal observer model with access to signals from 5,000 cones (see Methods for description). Points represent mean ± sem.

Chapter 4. CONE TYPE-SPECIFIC ADAPTATION

4.1 ABSTRACT

Adaptation matches neural gain to the prevailing inputs and allows the visual system to function over an impressive range of conditions. The degree to which this adaptation operates before or after the integration of inputs across different cones has strong implications for the interaction of signals from different cone types, and ultimately perception. Here, we record from primate parasol retinal ganglion cells to test the hypothesis that signals originating in different cone types adapt independently. Under the light conditions we tested, the gain in ganglion cells to signals originating in different cone types does indeed adapt independently. Cone type-specific gain control suggests that adaptation alters the gain to stimuli that are both chromatically and spatially similar to those invoking adaptation.

4.2 INTRODUCTION

Adaptation is the process by which sensory systems match their input-output relationships to their current inputs. An example is adaptation of gain in the visual system, by which the response per photon decreases as the mean stimulus intensity increases. This process has been studied starting with signal detection in the photoreceptors (Schneeweis & Schnapf, 1999; Dunn *et al.*, 2007; Angueyra & Rieke, 2013), throughout retinal, subcortical, and cortical circuits, and at the level of perception (Kohn, 2007).

Under daylight lighting conditions, signals in the visual system originate in 3 classes of photoreceptors with unique spectral sensitivities: long wavelength (L), medium wavelength (M), and short wavelength (S) cones. Very early in the retina, signals from different cone classes are pooled in convergent circuitry. With different spectral sensitivities, these cones respond to distinct,

albeit overlapping, sets of stimuli (Baylor *et al.*, 1987). Therefore, certain visual stimuli will activate them to a similar degree, while others will produce different activity levels in each cone type.

Does gain adaptation operate on signals from different cone classes before or after they are integrated by downstream neurons? In the first case, gain changes produced by high activity levels in one cone type would not affect the gain of signals from the other cone types, while in the second case, adaptational changes would act on signals from all cone types. Natural inputs have rich structure and therefore invoke a series of complex interactions between their different components. Uncovering whether adaptation operates on signals from different cone types together or separately is an important step in understanding the degree to which inputs of different wavelengths interact.

Past perceptual measurements have found evidence of adaptation occurring independently for stimuli targeting cones of different types (Mollon, 1982; Stockman & Mollon, 1986) and even for stimuli localized to individual cones across space (Macleod *et al.*, 1992). Direct cone recordings and electroretinograms suggest that cones do not adapt until background light levels exceeding those at which adaptation is first seen psychophysically (Schnapf *et al.*, 1990; Hood & Birch, 1993; Dunn *et al.*, 2007; Angueyra & Rieke, 2013; Cao *et al.*, 2014). Together these findings show that cone type-specific adaptation may occur under some but not all conditions.

Although adaptation has been studied at the level of retinal output signals, its degree of cone type-specificity has not been directly tested. Recordings from horizontal cells, which receive direct cone input, show cone type-specific adaptation (Lee *et al.*, 1999). Significant processing occurs between horizontal cells and the retinal output, thus it remains uncertain whether this cone type-specificity of adaptation persists in retinal ganglion cell responses. Parasol and peripheral

midget ganglion cells both integrate inputs across many cones of different spectral types. They exhibit gain adaptation via circuit-level mechanisms at dim light levels, but in the cones themselves at brighter light levels (Dunn *et al.*, 2007). This suggests that adaptation should occur in a cone type-specific manner at higher light levels. To begin to extend the results of Dunn et al., 2007, we recorded excitatory currents and spike responses in peripheral primate parasol ganglion cells and evaluated the cone-type specificity of gain adaptation. We found that adaptation indeed occurs in a cone type-specific manner.

4.3 RESULTS

Primate parasol ganglion cells provide an ideal location to test for cone type-specific adaptation. Parasol cells integrate signals from many L and M cones (Goodchild *et al.*, 1996). Further, at background light levels greater than ~1000 R*/s, adaptation in their response gain occurs primarily in the cones themselves, instead of within downstream circuitry (Dunn *et al.*, 2007). Do changes in the stimuli targeting one cone type affect the gain of parasol responses to inputs targeting the other?

To test for cone type-specific adaptation, we measured response gain to signals originating in either L or M cones at two different background light levels (Figures 4.1A and 4.1B). For either background, the M cone isomerization rate was held fixed at 4,000 R*/s. The L cone isomerization rate alternated between 4,000 R*/s for the first background and 12,000 R*/s for the second. These light levels were chosen because they are in a realm where parasol adaptation occurs within the cones and where cones show strong gain adaptation with increasing background isomerization rates (Figure 2.5; Angueyra and Rieke, 2013; Cao et al., 2014; Dunn et al., 2007). If cone type-specific adaptation occurs, we would expect the response gain for M cone isolating stimuli to remain unchanged between backgrounds because the average M cone input is fixed. Conversely,

we would expect the response gain for L cone signals to be lower on the background with a higher L cone isomerization rate. If cone type-specific adaptation does not occur, we would expect the response gains to signals originating in either cone type to change together. An intermediate case is also possible in which there is a shared adaptation component and a component specific to each cone type.

To measure gain of responses to signals from either cone type on each of the backgrounds, we recorded responses to cone-isolating Gaussian noise stimuli targeting either cone type at each background. Past work shows that adaptation can arise at the level of spike generation in ganglion cells (Kim & Rieke, 2001; Zaghloul, 2005; Beaudoin *et al.*, 2007). Thus, to gain insight into the site of any adaptation we observed, we measured adaptation in both excitatory currents and spike responses. For each recording type, we constructed a linear-nonlinear (LN) model for each of the four cases (Figures 4.1C and 4.1D). To make LN model linear filter amplitudes serve as a readout of relative gain, we aligned the models' nonlinearities by scaling their domains and applying the necessary scale factors to their filters (see Methods, Figures 4.1C and 4.1D, insets). After this alignment, the relative amplitudes of the linear filters served as a measure of relative gain under different background conditions.

Within each cell we compared adaptation between the two background light levels of the response gain for signals originating in L cones versus M cones (Figure 4.2). Backgrounds of 4,000 R*/s and 12,000 R*/s fall within the Weber range of cone adaptation (Angueyra & Rieke, 2013). Thus L cone gain would be expected to decrease by a factor of 3 at the higher background. In measurements of both excitatory currents (Figure 4.2A) and spikes (Figure 4.2B), L cone gain always adapted to a greater extent than M cone gain. In excitatory currents, the mean ± sem ratio of the gain on the higher background to that at lower background was 0.44 ± 0.08 in L cones and

0.95 ± 0.03 in M cones. In spike recordings, the ratio was 0.37 ± 0.04 in L cones and 1.01 ± 0.05 in M cones. These ratios agree quite well with the expected ratios of 0.33 in L cones and 1.0 in M cones if cone adaptation was Weber and adaptation was entirely cone type-specific.

4.4 DISCUSSION

Past work on the site of gain adaptation in the primate retina showed that it should occur in cone photoreceptors themselves at the light levels we tested (Dunn *et al.*, 2007). Adaptation at this site would be expected to produce cone type-specific adaptation in the gain of retinal ganglion cell responses, but this had not been directly tested. We find that adaptation in the gain of parasol ganglion cell responses indeed occurs in a cone type-specific manner.

Dunn et al., 2007 also showed that at dimmer light levels, the site of adaptation shifts to be within the retinal circuitry downstream of the cones. Because cone signals converge early in the retinal circuitry, circuit-level adaptation would be expected to affect the gain of signals from different cone types similarly. In further support of an absence of cone type-specific adaptation at lower light levels, cone photoreceptor recordings show minimal gain adaptation at lower light levels. It remains to be seen in future work if cone type-specific adaptation fails to occur at light levels lower than those we tested.

Whether cone types adapt independently or together has significant ramifications for perception. Natural inputs vary across many dimensions, such as space, time, and wavelength. There is precedent in the visual system for stimuli that vary across these different dimensions to interact with and influence the responses to one another, such as stimuli separated in space in a classic center-surround receptive field (Turner *et al.*, 2018). Adaptation that is not cone type-specific is an analogous example of a mechanism by which stimuli of one wavelength could shape responses to stimuli of another. Conversely, cone type-specific adaptation would increase the

degree of independence in the responses to signals originating in different cone types. Furthermore, it would have implications for color vision because shifts in the spectrum of illuminating light would cause differential adaptation in cones.

4.5 Future Directions

Significant efforts have been made to describe adaptation in cone photoreceptors, and there is a general consensus about how their response gain changes across background light levels (Angueyra and Rieke, 2013; Cao et al., 2014; Dunn et al., 2007; Schneeweis and Schnapf, 1999, Chapter 2). To what degree does cone adaptation control the gain of our perception? The work of Dunn et al., 2007 suggested that cone adaptation may control retinal output under certain conditions but not under others. Namely, the response gain of parasol and midget ganglion cells seems to adapt through a circuit-level mechanism at lower light levels and via changes in cones themselves at higher light levels. Our demonstration of cone type-specific adaptation supports the role of cones in controlling adaptation at higher light levels. A logical next step would be to evaluate cone type-specific adaptation at dimmer light levels when adaptation is presumed to occur within circuitry downstream of the cones. This could both further validate the model of multiple sites of adaptation as well as expand our understanding of the conditions under which cone gain controls the gain of the retinal output.

Dunn et al. 2007 suggest that convergence of signals from many cones contributes to the ability of circuit-level mechanisms to implement reliable adaptational changes at lower light levels. We find minimal differences in adaptation in cones across eccentricity (data not shown). In central retina, where midget ganglion cells receive single cone input, do circuit level mechanisms still control gain at lower light levels? Or, does an absence of convergence result in cone gain controlling the gain of the retinal output across all light levels? It will be important to answer

questions such as these to determine the implications for perception of our findings in cones themselves. The validation of cone type-specific adaptation presented in this chapter is the beginning of our work to address these questions.

4.6 METHODS

4.6.1 *Tissue, cells, and solutions*

Electrophysiological recordings were performed in primate retina from the Tissue Distribution Program of the University of Washington's Regional Primate Research Center. Recordings were made from retinas from *Macaca fascicularis, Macaca nemestrina,* and *Macaca mulatta* aged 2 through 20 years, of both sexes. All primate tissue use was completed in accordance with the University of Washington Institutional Animal Care and Use Committee. Tissue was obtained and prepared as described previously (Angueyra & Rieke, 2013; Sinha *et al.*, 2017). In short, dark adapted (> 1 hour) retina stored in warm (32° C), oxygenated Ames medium was placed photoreceptor side down on a poly-lysine-coated coverslip (BD Biosciences) that served as the floor of our recording chamber. The tissue was continuously perfused throughout recordings with warm, oxygenated Ames solution.

4.6.2 *Patch-clamp recordings*

Recordings were performed as described previously (Sinha *et al.*, 2017). All data were low-pass filtered at 3 kHz, digitized at 10 kHz, and acquired using a Multiclamp 700B amplifier. Recordings were controlled using Symphony Data Acquisition software, a piece of MATLAB-based, open-source electrophysiology software (https://github.com/symphony-das).

4.6.3 *Light stimulation*

All stimulus protocols were generated using custom-written extensions of Symphony Data Acquisition Software and delivered from computer-driven LEDs with peak wavelengths of 406, 515, and 640 nm. This allowed effective stimulation of all 3 cone types. Light stimuli were centered on the cell being recorded from and covered a ~500 μm disk. Isomerization rates were calculated from LED power output measurements, measured LED spectra, primate cone spectra from Baylor et al., 1987 and a cone collecting area of 0.37 μm^2 (Schnapf *et al.*, 1990). These rates were used to construct a matrix mapping from LED output to isomerizations in each cone type. The inverse of this matrix mapped from cone isomerizations to LED output, and was used to set cone type-specific background light levels as well as generate cone-isolating stimuli.

4.6.4 *Analysis*

All data were analyzed using custom-written MATLAB analysis routines.

LN Model Construction: Linear-nonlinear (LN) models were constructed as described previously (Kim & Rieke, 2001). In the case of excitatory current recordings, target LN model outputs for fitting were taken to be the recorded currents. In the case of spike recordings, they were binary vectors with a 1 at each spike time and 0's elsewhere.

Gain comparison: LN models were used to compare a cell's gain under different input conditions. The amplitude of a linear filter in an LN model is only meaningful in the context of the scale of the inputs to the nonlinear function. For example, if the same scale factor is used to scale an LN model's linear filter as well as the domain of its static nonlinearity, the transformation represented by the model remains the same. When the gains in LN models from multiple conditions are being compared, their nonlinearities can be aligned by scaling their input values. If the same factors are applied to all of the respective linear filters, the transformations of the models remain

unchanged. Once the nonlinearities are aligned, differences in the amplitudes of the linear filters become directly relatable to relative differences in gain because all of the filters are producing a generator signal that will be put into the same, aligned, nonlinearity. We used this approach to calculate the relative gains of ganglion cells to cone-isolating stimuli at different background light levels.

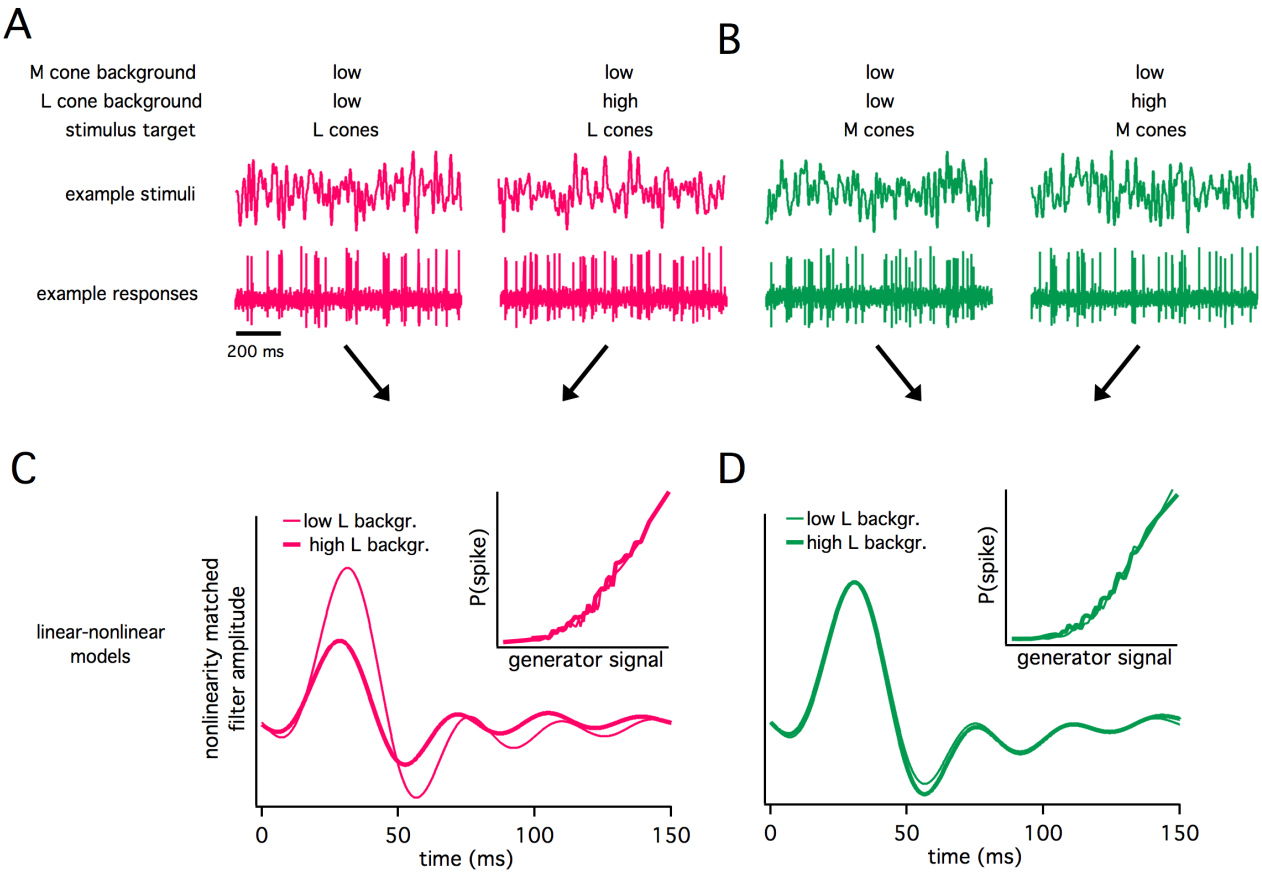

Figure 4.1. Cone type-specific adaptation analysis

(A) Top traces show example cone-isolating Gaussian noise stimuli (in units of contrast) isolating L cones on a background with a mean isomerization rate of 4,000 R*/s in M cones and 4,000 R*/s in L cones (left) or 4,000 R*/s in M cones and 12,000 R*/s in L cones (right). Bottom shows example spike responses from a parasol retinal ganglion cell to example stimuli.

(B) Data from same cell and backgrounds as in (A), but for Gaussian noise stimuli isolating M cones.

(C) Linear-nonlinear models for L cone-isolating stimuli in example cell from (A) and (B). Linear filters show relative gain to L cone-isolating stimuli on backgrounds with lower (thin line) or higher (thick line) L cone mean isomerization rates. Inset shows aligned nonlinearities for

models fit to data at either background, which allows filter amplitudes to serve as a measure of relative gain.

(D) As in (C), but for M cone-isolating stimuli on low or high L cone isomerization rate backgrounds.

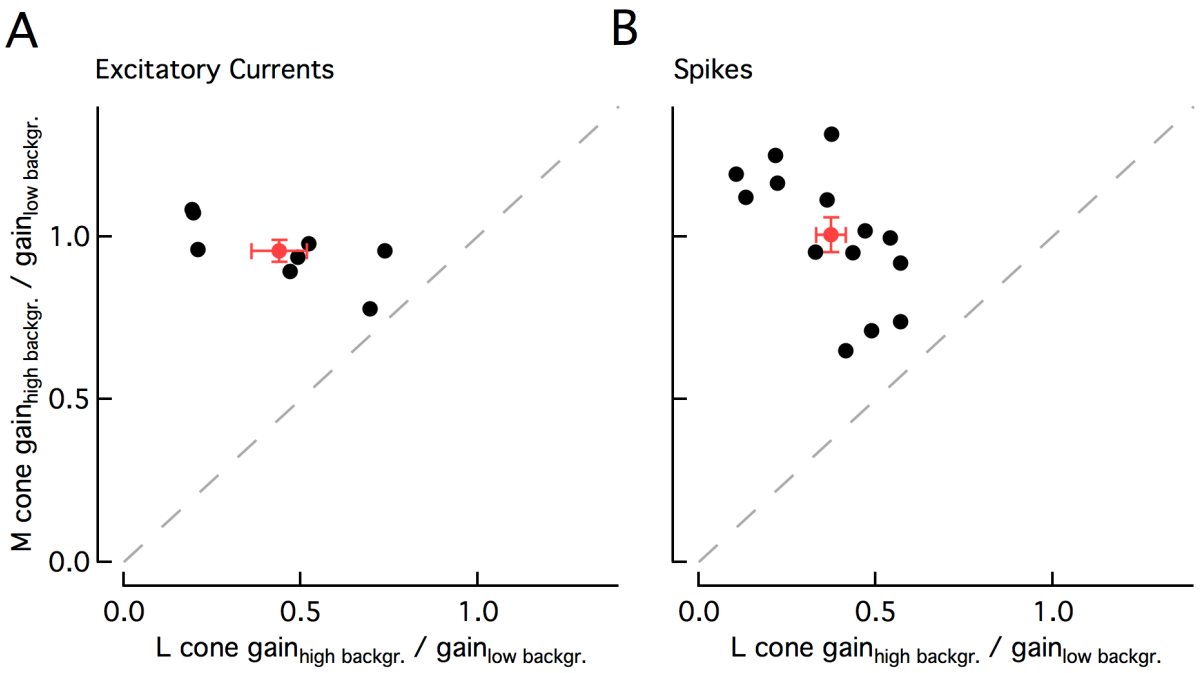

Figure 4.2. Cones adapt independently

(A) Ratio of L cone gain on higher background (M: 4,000 R*/s; L: 12,000 R*/s) to that on lower background (M: 4,000 R*/s; L: 4,000 R*/s) versus the ratio of M cone gain at the same backgrounds in excitatory currents of parasol ganglion cells. L cone gain adapted significantly more than M cone gain ($p < 0.005$, paired t-test). Gains were computed from linear-nonlinear (LN) model fits to responses to cone-isolating stimuli at each background (see Methods).

(B) As in (A), but for gain calculated from LN models fit to spike data from parasol ganglion cells. L cone gain adapted significantly more than M cone gain ($p < 10^{-5}$, paired t-test).

Chapter 5. CONCLUDING REMARKS

Understanding and explaining human visual perception has been a shared goal of centuries of psychophysical and physiological work in the visual system. A complete understanding will allow human perception to be explained at the level of the computations performed by the cells and neural circuits that comprise the visual system. Significant progress has been made toward this end. Visual processing commences in the very first neurons of the visual system, cone photoreceptors. Signals generated in cones are fed into a diverse array of parallel pathways within the retina. It has long been appreciated that the retina's parallel architecture affords it the ability to implement a range of different computations (Field & Chichilnisky, 2007). Thus, different computations have been associated with different circuitry. Interestingly this appreciation of heterogeneity has not been extended to cone photoreceptors, which are commonly assumed to be functionally homogeneous when attempting to explain retinal output or perception. Work presented in this thesis describes previously unappreciated heterogeneity in primate cone photoreceptors as well as demonstrates or predicts manners in which cone properties directly control the retinal output and ultimately perception.

5.1 WHAT HETEROGENEITY EXISTS IN PRIMATE CONES?

Differences we find in cones across spectral type and eccentricity provide direct evidence against the assumption that primate cones are functionally homogenous across the retina. Our findings motivate future work in primate cones, revision of previous interpretations of physiological and psychophysical results, and incorporation of our findings into future models of the visual system.

5.1.1 *Cone differences across spectral type*

Chapter 2 presents previously unrecognized differences in cones across spectral types. We describe three main findings: (1) S cones have slower kinetics compared to L and M cones; (2) unlike L and M cones, S cone kinetics change minimally over background light levels; and (3) at lower backgrounds, S cones are noisier than L and M cones, leading to increased detection thresholds. To reach these conclusions we evaluated multiple cone properties across a range of background light levels, but this far from exhausts the inputs encountered by primate cones. Follow-up work should aim to expand our understanding of cone heterogeneity by extending the set of inputs over which comparisons are made between cones across spectral types.

Cone differences are most relevant in the context of the actual inputs our visual systems encounter. Recent work has emphasized the importance of studying the retina's response to natural inputs (Heitman *et al.*, 2016; Turner & Rieke, 2016; Turner *et al.*, 2018). Related to this, there are two main extensions of the work in Chapter 2 that would be particularly salient. First, we compared S cone response properties to L and M cones across background light levels spanning 2 orders of magnitude, while cones provide the dominant input to the visual system over a much broader range. How do their responses vary over this entire range? Comparisons should be made between cones of different spectral type across a larger range of background light levels. Second, under natural conditions, saccades and other eye movements cause cone inputs to rapidly change. Thus, cones are constantly updating their signaling properties to match their prevailing inputs. We measured cone response properties across different stimulus conditions, but only after cones had adapted to those conditions. This adaptation has its own timescale. Therefore, immediately following a change in light level, cone properties will be at an intermediate point between the steady state elicited by their previous inputs and that of their new inputs. Because natural cone

inputs change on a rapid timescale, the dynamics of this adaptation are perceptually relevant. Therefore, future work on cone differences should extend beyond steady state differences and also characterize the temporal dynamics of the transitions between these states.

Differences between L and M cones and S cones add a previously unappreciated wavelength dependence to our understanding of visual perception. Decades of work demonstrates that signals originating in S cones have properties distinct from those originating in L or M cones, both within downstream cells of the visual system and in perception (Brindley *et al.*, 1966; Stockman *et al.*, 1993; Cottaris & De Valois, 1998; Tailby *et al.*, 2008; Smithson, 2014). To gain insight into the underlying mechanisms, these differences are often related to models of visual system circuitry. To what degree do they originate in cones themselves? Our findings suggest that such circuit models must begin with validated models of cone responses that capture differences in cones across the retina. Significant efforts have been made to construct biophysically motivated photoreceptor models (Rieke & Baylor, 1998; Korenbrot, 2012). It will be important to fit distinct models to the responses of cones of each spectral type. This will have two main benefits: (1) accurate cone models will help differentiate between the role of cones and downstream circuit elements in shaping perception; and (2) biophysical models can begin to provide insight into the mechanistic basis of the differences between cone types. In preliminary attempts to do this, we found that time constraints on regular whole-cell patch clamp recordings from cones were restrictive by limiting the amount of data that could be collected. This decreases the generalizability of models fit using these data. It may be possible to overcome this constraint by collecting data using an alternative approach, such as perforated patch clamp.

The constancy of S cone kinetics across background light levels provides a potential experimental tool. When interpreting psychophysical measurements or recordings from neurons

downstream in the visual system, it is often difficult to determine if differences in S cone pathways arise within S cones themselves or downstream circuitry. Our recordings demonstrate that kinetic differences between L and M cones and S cones increase with increasing background light level. This finding makes direct predictions about how differences in downstream responses or perception of signals originating in different cone types should vary with light level, if the variability is attributable to differences in the cones themselves. Our evaluation of the role of S cone properties in the responses of small bistratified ganglion cells in Chapter 2 was based on this approach. It would be interesting to revisit classic S cone psychophysics experiments such as Benham's top (von Campenhausen & Schramme, 1995) or those of Stockman et al., 1993 to determine if perception across background light levels changes in a manner predicted by differences in the cones themselves.

5.1.2 *Cone differences across eccentricity*

Chapter 3 elaborates on previously reported differences in cones across space (Sinha *et al.*, 2017). Three main differences across eccentricity are: (1) cone kinetics accelerate in a graded manner with increasing eccentricity; (2) kinetic differences across eccentricity persist across a range of background light levels; and (3) foveal cones transmit less information than peripheral cones, especially at high frequencies. Signals generated in foveal retina, providing our highest spatial and chromatic acuity, are arguably the most important inputs to our visual system. Thus, it is essential to develop a comprehensive understanding how signal detection in the central-most retina varies from that in the more commonly studied peripheral retina. Our understanding of cone differences across eccentricity will be further advanced by follow-up work similar to that proposed for S cones versus L and M cones. Namely, differences in foveal, central, and peripheral cones should be evaluated across a broader range of light levels. Further, the timescales of changes in cone

properties should be compared across eccentricity. The persistence in voltage clamp of foveal versus peripheral kinetic differences suggests they originate at the level of phototransduction (Sinha *et al.*, 2017). Phototransduction will also control timescales of adaptation. Given that phototransduction in foveal cones is different enough to produce a ~2-fold kinetic difference in their light responses, it would be unsurprising if it also had a major effect on timescales of adaptation.

As with differences in cones across spectral type, it will be important to incorporate the differences we find in cones across eccentricity into retinal models. Such models will help us better understand the implications cone differences have for responses downstream in the retina. For example, midget ganglion cells in central retina receive inputs from single cones, while those in the periphery integrate across many cones. Given that foveal cones already transmit less information than their peripheral counterparts, what does this mean for the levels of information present in foveal versus peripheral ganglion cells?

Eccentricity is one measure of cone location across visual space. It would be interesting to see if cones vary along other dimensions. For example, are cones in temporal retina different from those in nasal retina, or dorsal retina versus ventral retina? Such differences are not without precedent in mammalian retina. For example, in mouse, there is a graded change in opsin expression across the dorsal-ventral axis (Szél *et al.*, 1996). Although such obvious biochemical differences have not been observed in primate retina, our findings here warrant heightened caution moving forward about additional heterogeneity in cone properties.

A final remaining question regarding kinetic differences across eccentricity relates to their origin. Is there an advantage to having foveal responses be slower or peripheral responses be faster? Does something about the combination of the timescales of eye movements in primates and

natural scene statistics make the kinetic gradient we observe improve the encoding of visual inputs? Or alternatively, are foveal cones slower out of necessity? High cone density in the central-most retina requires the structure of foveal cones to be distinct from that of peripheral cones. For example, foveal cone axons may be up to ~400 μm in length, while peripheral cone axons are significantly shorter (Hsu *et al.*, 1998). Such differences could alter the fidelity of signal transfer down foveal cone axons. Did slower foveal cones somehow develop as a necessary trade-off to accommodate these structural differences that allow high cone density and therefore increased spatial acuity? Answers to these questions may come from two sources. A better understanding of the mechanistic basis of the kinetic differences may provide insight into whether having slower foveal kinetics was an evolutionary trade-off. Building models of visual encoding using cone responses, timescales of eye movements, and known natural visual input properties would help address the role of slower foveal kinetics in the encoding of natural inputs.

5.2 When do cone properties control retinal output and predict perception?

Predictions of flicker fusion frequencies from models we constructed incorporating differences in cones across eccentricity were well aligned with perceptual measurements. Numerous synapses and significant processing occurs between cone photoreceptors and perception, meaning perceptual differences across eccentricity could have easily existed in the absence of differences in cones themselves. But in the case of flicker fusion, cone properties appear likely to contribute strongly to perceptual differences across eccentricity. Similarly, in Chapter 2, we showed that differences in how S cone versus L and M cone response kinetics adapt across background light levels are directly observable in the responses of small bistratified ganglion cells. This demonstrates another instance in which cone properties control downstream

responses. Conversely, the kinetics of peripheral parasol and midget ganglion cell responses did not follow kinetic changes observed the cone types providing their main inputs (data not shown). The contrast between these instances demonstrates why caution must be taken when interpreting the properties of cone photoreceptors. Because their signals traverse a myriad of downstream pathways, it is important to pair findings about cone properties to either direct downstream recordings and psychophysical measurements, or models attempting to relate observed cone properties to known aspects of perception.

BIBLIOGRAPHY

Angueyra JM & Rieke F (2013). Origin and effect of phototransduction noise in primate cone photoreceptors. *Nat Neurosci* **16,** 1692–1700.

Barlow HB (1957). Purkinje shift and retinal noise. *Nature* **179,** 255–256.

Barrow AJ & Wu SM (2009). Low-Conductance HCN1 Ion Channels Augment the Frequency Response of Rod and Cone Photoreceptors. *J Neurosci* **29,** 5841–5853.

Baylor D (1996). How photons start vision. *Proc Natl Acad Sci U S A* **93,** 560–565.

Baylor DA, Lamb TD & Yau KW (1979). Responses of retinal rods to single photons. *J Physiol* **288,** 613–634.

Baylor DA, Nunn B & Schnapf J (1984). The photocurrent, noise, and spectral sensitivities of rods of the monkey Macaca fascicularis. *J Physiol* **357,** 575–607.

Baylor DA, Nunn BJ & Schnapf JL (1987). Spectral sensitivity of cones of the monkey Macaca fascicularis. *J Physiol* **390,** 145–160.

Beaudoin DL, Borghuis BG & Demb JB (2007). Cellular Basis for Contrast Gain Control over the Receptive Field Center of Mammalian Retinal Ganglion Cells. *J Neurosci* **27,** 2636–2645.

Bialek W, DeWeese M, Rieke F & Warland D (1993). Bits and brains: Information flow in the nervous system. *Phys A Stat Mech its Appl* **200,** 581–593.

Bialek W, Rieke F, de Ruyter van Steveninck R & Warland D (1991). Reading a neural code. *Science (80-)* **252,** 1854–1857.

Brindley GS, Du Croz JJ & Rushton WAH (1966). The Flicker Fusion Frequency of the Blue-

Sensitive Mechanism of Colour Vision. *J Physiol* **183,** 497–500.

Calkins DJ, Tsukamoto Y & Sterling P (1998). Microcircuitry and mosaic of a blue-yellow ganglion cell in the primate retina. *J Neurosci* **18,** 3373–3385.

von Campenhausen C & Schramme J (1995). 100 Years of Benham Top in Color Science. *Perception* **24,** 695–717.

Cao L-H, Luo D-G & Yau K-W (2014). Light responses of primate and other mammalian cones. *Proc Natl Acad Sci* **111,** 2752–2757.

Cottaris NP & De Valois RL (1998). Temporal dynamics of chromatic tuning in macaque primary visual cortex. *Nature* **395,** 896–900.

Crook JD, Davenport CM, Peterson BB, Packer OS, Detwiler PB & Dacey DM (2009). Parallel ON and OFF cone bipolar inputs establish spatially coextensive receptive field structure of blue-yellow ganglion cells in primate retina. *J Neurosci* **29,** 8372–8387.

Dacey DM & Lee BB (1994). The "blue-on" opponent pathway in primate retina originates from a distince bistratified ganglion cell type. *Nature* **367,** 731–735.

Donner K (1992). Noise and the Absolute Thresholds of Cone and Rod Vision. *Vision Res* **32,** 853–866.

Duda RO, Hart PE & Stork DG (2001). *Pattern classification*, 2nd edn. Wiley, New York.

Dunn F a, Lankheet MJ & Rieke F (2007). Light adaptation in cone vision involves switching between receptor and post-receptor sites. *Nature* **449,** 603–606.

Fairhall AL, Lewen GD & Bialek W (2001). Eficiency and ambiguity in an adaptive neural code. *Nature*.

Field GD & Chichilnisky EJ (2007). Information processing in the primate retina: circuitry and coding. *Annu Rev Neurosci* **30,** 1–30.

Field GD, Sampath AP & Rieke F (2005). Retinal processing near absolute threshold: from behavior to mechanism. *Annu Rev Physiol* **67,** 491–514.

Field GD, Sher A, Gauthier JL, Greschner M, Shlens J, Litke AM & Chichilnisky EJ (2007). Spatial properties and functional organization of small bistratified ganglion cells in primate retina. *J Neurosci* **27,** 13261–13272.

Geisler WS (1989). Sequential Ideal-Observer Analysis of Visual Discriminations. *Psychol Rev* **96,** 267–314.

Goodchild AK, Ghosh KK & Martin PR (1996). Comparison of photoreceptor spatial density and ganglion cell morphology in the retina of human, macaque monkey, cat, and the marmoset Callithrix jacchus. *J Comp Neurol* **366,** 55–75.

Green DG (1969). Sinusoidal flicker characteristics of the color-sensitive mechanisms of the eye. *Vision Res* **9,** 591–601.

Hass CA, Angueyra JM, Lindbloom-Brown Z, Rieke F & Horwitz GD (2015). Chromatic detection from cone photoreceptors to V1 neurons to behavior in rhesus monkeys. *J Vis* **15,** 1.

Hecht S (1942). Energy, Quanta, and Vision. *J Gen Physiol* **25,** 819–840.

Hecht S & Shlaer S (1936). Intermittent Stimulation by Light. *J Gen Physiol* **19,** 965–977.

Hecht S & Verrijp CD (1933). Intermittent Stimulation By Light III. The Relation Between Intensity and Critical Fusion Frequency for Different Retinal Locations. *J Gen Physiol* **17,** 251–268.

Heitman A, Brackbill N, Greschner M, Sher A, Litke AM & Chichilnisky EJ (2016). Testing pseudo-linear models of responses to natural scenes in primate retina. *bioRxiv* **17992,** 1–20.

Hood DC & Birch DD (1993). Human cone receptor activity: The leading edge of the a-wave

and models of receptor activity. *Vis Neurosci* **10,** 857–871.

Hornstein EP, Verweij J & Schnapf JL (2004). Electrical coupling between red and green cones in primate retina. *Nat Neurosci* **7,** 745–750.

Howlett MHC, Smith RG & Kamermans M (2017). A novel mechanism of cone photoreceptor adaptation. *PLoS Biol* **15,** 1–28.

Hsu A, Tsukamoto Y, Smith RG & Sterling P (1998). Functional architecture of primate cone and rod axons. *Vision Res* **38,** 2539–2549.

Kandel ER, Schwartz JH, Jessel TM, Siegelbaum SA & Hudspeth AJ (2013). *Principles of Neural Science*, 5th edn. McGraw-Hill Education.

Kim KJ & Rieke F (2001). Temporal contrast adaptation in the input and output signals of salamander retinal ganglion cells. *J Neurosci* **21,** 287–299.

Koenig D & Hofer H (2011). The absolute threshold of cone vision. *J Vis* **11,** 1–24.

Kohn A (2007). Visual Adaptation: Physiology, Mechanisms, and Functional Benefits. *J Neurophysiol* **10461,** 3155–3164.

Korenbrot JI (2012). Speed, adaptation, and stability of the response to light in cone photoreceptors: the functional role of Ca-dependent modulation of ligand sensitivity in cGMP-gated ion channels. *J Gen Physiol* **139,** 31–56.

Laughlin S (1981). A Simple Coding Procedure Enhances a Neuron's Information Capacity. *Zeitschrift fur Naturforsch* **36,** 910–912.

Lee BB, Dacey DM, Smith VC & Pokorny J (1999). Horizontal cells reveal cone type-specific adaptation in primate retina. *Proc Natl Acad Sci* **96,** 14611–14616.

Lee RJ, Mollon JD, Zaidi Q & Smithson HE (2009). Latency characteristics of the short-wavelength-sensitive cones and their associated pathways. *J Vis* **9,** 5.1-17.

Luo D-G, Yue WWS, Ala-Laurila P & Yau K-W (2011). Activation of Visual Pigments by Light and Heat. *Science (80-)* **332,** 1307–1313.

Macleod DIA, Williams DR & Makous W (1992). A visual nonlinearity fed by single cones. *Vision Res* **32,** 347–363.

Mante V, Frazor RA, Bonin V, Geisler WS & Carandini M (2005). Independence of luminance and contrast in natural scenes and in the early visual system. *Nat Neurosci* **8,** 1690–1697.

Marks LE & Bornstein MH (1973). Spectral sensitivity by constant CFF: effect of chromatic adaptation. *J Opt Soc Am* **63,** 220–226.

Miller J, Picones A & Korenbrot J (1994). Differences in transduction between rod and cone photoreceptors: an exploration of the role of calcium homeostasis. *Curr Opin Neurobiol* **4,** 488–495.

Mollon JD (1982). Color Vision. *Annu Rev Psychol* **33,** 41–85.

Nathans J, Thomas D & Hogness DS (1986). Molecular Genetics of Human Color Vision: The Genes Encoding Blue, Green, and Red Pigments. *Science (80-)* **232,** 195.

Packer OS, Verweij J, Li PH, Schnapf JL & Dacey DM (2010). Blue-yellow opponency in primate S cone photoreceptors. *J Neurosci* **30,** 568–572.

Pokorny J & Smith VC (1970). Wavelength Discrimination in the Presence of Added Chromatic Fields. *J Opt Soc Am* **60,** 562–569.

Rieke F & Baylor D (1998). Single-photon detection by rod cells of the retina. *Rev Mod Phys* **70,** 1027–1036.

Rieke F & Baylor DA (2000). Origin and Functional Impact of Dark Noise in Retinal Cones. *Neuron* **26,** 181–186.

Rieke F, Warland D & Bialek W (1993). Coding efficiency and information rates in sensory

neurons. *Europhys Lett* **22,** 151–156.

Rieke F, Warland D, de Ruyter van Steveninck R & Bialek W (1997). *Spikes: Exploring the Neural Code*. MIT Press, Cambridge, MA, USA.

Ronnett G V. & Moon C (2002). G Proteins and Olfactory Signal Transduction. *Annu Rev Physiol* **64,** 189–222.

Sanes JR & Masland RH (2015). The Types of Retinal Ganglion Cells: Current Status and Implications for Neuronal Classification. *Annu Rev Neurosci* **38,** 221–246.

Santina L Della, Piano I, Cangiano L, Caputo A, Ludwig A, Cervetto L & Gargini C (2012). Processing of retinal signals in normal and HCN deficient mice. *PLoS One* **7,** 1–10.

Schnapf JL, Nunn BJ & Baylor DA (1990). Visual transduction in cones of the monkey Macaca fascicularis. *J Physiol*681–713.

Schneeweis DM & Schnapf JL (1999). The photovoltage of macaque cone photoreceptors: adaptation, noise, and kinetics. *J Neurosci* **19,** 1203–1216.

Seiple W & Holopigian K (1996). Outer-retina locus of increased flicker sensitivity of the peripheral retina. *J Opt Soc Am* **13,** 658–666.

Shannon CE (1949). Communication In The Presence Of Noise. *Proc Inst Radio Eng* **37,** 10–21.

Shevell SK (2003). *The Science of Color, second edition*, 2nd edn.ed. Shevell SK. Elsevier, Oxford, UK.

Sinha R, Hoon M, Baudin J, Okawa H, Wong ROL, Rieke F, Sinha R, Hoon M, Baudin J, Okawa H, Wong ROL & Rieke F (2017). Cellular and Circuit Mechanisms Shaping the Perceptual Properties of the Primate Fovea Article Cellular and Circuit Mechanisms Shaping the Perceptual Properties of the Primate Fovea. *Cell* **168,** 413–426.e12.

Smithson HE (2014). S-cone psychophysics. *Vis Neurosci* **31,** 211–225.

Smithson HE & Mollon JD (2004). Is the S-opponent chromatic sub-system sluggish? *Vision Res* **44,** 2919–2929.

Snowden RJ & Hess RF (1992). Temporal frequency filters in the human peripheral visual field. *Vision Res* **32,** 61–72.

Solomon SG, Martin PR, White AJR, Rüttiger L & Lee BB (2002). Modulation sensitivity of ganglion cells in peripheral retina of macaque. *Vision Res* **42,** 2893–2898.

Stockman A, MacLeod DIA & DePriest DD (1991). The temporal properties of the human short-wave photoreceptors and their associated pathways. *Vision Res* **31,** 189–208.

Stockman A, MacLeod DIA & Lebrun S (1993). Faster than the eye can see: blue cones respond to rapid flicker. *J Opt Soc Am* **10,** 1396–1402.

Stockman A & Mollon JD (1986). The Spectral Sensitivities of the Middle-Wavelength and Long-Wavelength Cones - an Extension of the 2-Color Threshold Technique of Stiles,W.S. *Perception* **15,** 729–754.

Stockman A & Sharpe LT (2000). The spectral sensitivities of the middle- and long-wavelength-sensitive cones derived from measurements in observers of known genotype. *Vision Res* **40,** 1711–1737.

Szél Á, Röhlich P, Caffé AR & Van Veen T (1996). Distribution of cone photoreceptors in the mammalian retina. *Microsc Res Tech* **35,** 445–462.

Tailby C, Solomon SG & Lennie P (2008). Functional asymmetries in visual pathways carrying S-cone signals in macaque. *J Neurosci* **28,** 4078–4087.

Tinsley JN, Molodtsov MI, Prevedel R, Wartmann D, Espigulé-Pons J, Lauwers M & Vaziri A (2016). Direct detection of a single photon by humans. *Nat Commun*; DOI: 10.1038/ncomms12172.

Turner MH & Rieke F (2016). Synaptic Rectification Controls Nonlinear Spatial Integration of Natural Visual Inputs. *Neuron* **90,** 1257–1271.

Turner MH, Schwartz GW & Rieke F (2018). Receptive field center-surround interactions mediate context-dependent spatial contrast encoding in the retina. *bioRxiv*252148.

Tyler CW (1987). Analysis of visual modulation sensitivity. III. Meridional variations in peripheral flicker sensitivity. *J Opt Soc Am* **4,** 1612.

Valeton JM & van Norren D (1983). Light Adaptation of Primate Cones : an Analysis Based on Extracellular Data. *Vision Res* **23,** 1539–1547.

Wässle H, Grünert U, Röhrenbeck J & Boycott BB (1989). Cortical magnification factor and the ganglion cell density of the primate retina. *Nature* **342,** 643–646.

Wiener N (1949). *Extrapolation, interpolation, and smoothing of stationary time series, with engineering applications*.

Yau K-W & Hardie RC (2009). Phototransduction motifs and variations. *Cell* **139,** 246–264.

Zaghloul KA (2005). Contrast Adaptation in Subthreshold and Spiking Responses of Mammalian Y-Type Retinal Ganglion Cells. *J Neurosci* **25,** 860–868.

Zhaoping L, Geisler WS & May KA (2011). Human wavelength discrimination of monochromatic light explained by optimal wavelength decoding of light of unknown intensity. *PLoS One*; DOI: 10.1371/journal.pone.0019248.

VITA

Jacob Baudin was born in Puyallup, Washington. He attended the University of Washington for his undergraduate studies. In 2012, he graduated with a Bachelor of Science and a Bachelor of Art with majors in Neurobiology, Philosophy, Biochemistry, and Biology. Jacob then entered the MD/PhD program at the University of Washington, where he completed his first two years of medical school before joining the lab of Fred Rieke in 2014. He completed his doctorate in Physiology & Biophysics in 2018. Outside of science, his interests are cooking, baking, travel, and exercise, especially when done with others.